

**Numerical analysis of a solar air heater  
having rectangular sectioned V-ribs as  
artificial roughness integrated with  
impingement cooling configuration**



**By**

**Muhammad Haroon Iqbal**

**Reg # 00000330579**

**Session 2020-2022**

**Supervised by**

**Dr. Majid Ali**

**MASTER OF SCIENCE in  
Thermal Energy Engineering**

**U.S-Pakistan Center for Advanced Studies in Energy (USPCAS-E)**

**National University of Sciences and Technology (NUST)**

**H-12, Islamabad 44000, Pakistan**

**January 2023**

## **THESIS ACCEPTANCE CERTIFICATE**

Certified that final copy of MS/MPhil thesis written by Muhammad Haroon Iqbal (Registration No. 00000330579), of U.S.-Pakistan Centre for Advanced Studies in Energy has been vetted by undersigned, found complete in all respects as per NUST Statues/Regulations, is within the similarity indices limit and accepted as partial fulfillment for the award of MS/MPhil degree. It is further certified that necessary amendments as pointed out by GEC members of the scholar have also been incorporated in the said thesis.

Signature: \_\_\_\_\_

Name of Supervisor: Dr. Majid Ali

Date: \_\_\_\_\_

Signature (HoD): \_\_\_\_\_

Date: \_\_\_\_\_

Signature (Dean/Principal): \_\_\_\_\_

Date: \_\_\_\_\_

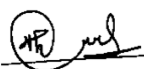
## Certificate

This is to certify that work in this thesis has been carried out by **Mr. Muhammad Haroon Iqbal** and completed under my supervision in, US-Pakistan Center for Advanced Studies in Energy (USPCAS-E), National University of Sciences and Technology, H-12, Islamabad, Pakistan.

Supervisor:

\_\_\_\_\_  
Dr. Majid Ali  
USPCAS-E  
NUST, Islamabad

Co-Supervisor:

\_\_\_\_\_  
  
Dr. Naveed Ahmed  
USPCAS-E  
NUST, Islamabad

GEC member 1:

\_\_\_\_\_  
Dr. Adeel Waqas  
USPCAS-E  
NUST, Islamabad

GEC member 2:

\_\_\_\_\_  
Dr. Mariam Mahmood  
USPCAS-E  
NUST, Islamabad

GEC member 3:

\_\_\_\_\_  
Dr. Muhammad Bilal Sajid  
USPCAS-E  
NUST, Islamabad

HOD-TEE:

\_\_\_\_\_  
Dr. Majid Ali  
USPCAS-E  
NUST, Islamabad

Dean/Principal:

\_\_\_\_\_  
Dr. Adeel Waqas  
USPCAS-E  
NUST, Islamabad

## **Dedication**

To my beloved parents (Mr. Muhammad Iqbal and Ms. Khalida Iqbal) who has always believed in me and inspired me to follow my dreams, and without their constant motivation, this work would not have been possible.

## Abstract

The application of solar air heaters (SAHs) is an effective method of utilizing abundant solar energy for heating purposes and reducing the consumption of fossil fuels. However, the performance of SAHs is characteristically low owing to a sublayer formation over the heated surface. To address this low performance, numerical examinations on a novel configuration of SAH have been performed in this study. The proposed design encompasses a combined arrangement of both impinging air jets and rectangular sectioned V-ribs on the absorber surface. A validated numerical model is used to investigate the effect of varying roughness height, pitch, and angle of attack from 0.016 to 0.024, 0.264 to 0.792, and  $30^\circ$  to  $75^\circ$  respectively while keeping impingement parameters fixed and varying Re from 3000 to 18000. The analysis results in terms of Nusselt number (Nu) and friction factor (ff) characteristics as a function of roughness parameters are evaluated. The results exhibit a considerable enhancement of 3.36 and 5.31 in Nu and ff respectively in contrast to conventional SAHs under similar boundary conditions. Moreover, the proposed model performs best at Re = 18000 with the highest thermohydraulic performance ( $\eta_{\text{combined}}$ ) of 1.92. The presented results conclude that the proposed arrangement of jet cooling with rectangular sectioned V-ribs is an efficacious way for improving the performance of SAHs.

**Keywords:** Solar Air Heater, Heat Transfer Enhancement, Impingement Heat Transfer, Computational Fluid Dynamics, Nusselt Number, Friction Factor

## Table of Contents

Abstract .....	IV
Table of Contents .....	V
List of Figures .....	VII
List of Tables .....	VIII
List of Publications .....	IX
List of Nomenclature .....	X
Chapter 1 Introduction .....	1
1.1. Background .....	1
1.2. Principle .....	3
1.3. Problem Statement .....	4
1.4. Research Objectives .....	5
1.5. Scope and Limitations .....	5
1.5.1. Scope .....	5
1.5.2. Limitations .....	5
1.6. Organization of thesis .....	6
Summary .....	7
References .....	8
Chapter 2 Literature Review .....	11
2.1. Augmentation Techniques .....	11
2.2. Artificial Roughness .....	11
2.3. Impingement Technique .....	14
2.4. Air Impingement with Artificial Roughness – A Combined Technique ....	16
2.5. Research Gap .....	17
Summary .....	18
References .....	19
Chapter 3 Methodology .....	23

3.1. Model Creation.....	23
3.1.1. Geometry Creation.....	23
3.1.2. Computational Domain and Mesh Generation .....	26
3.2. Grid Independence Study .....	27
3.3. Turbulence Model .....	28
3.4. Governing Equations.....	28
3.5. Boundary conditions and solution methods .....	29
Summary .....	31
References.....	32
Chapter 4 Results and Discussions .....	33
4.1. Validation of the numerical model.....	33
4.1.1. Validation with smooth rectangular air channel .....	33
4.1.2. Validation with impinging air jets onto a smooth absorber .....	33
4.2. Effect on temperature distribution.....	35
4.3. Effect on Nusselt number .....	36
4.4. Effect on friction factor .....	41
4.5. Effect on thermohydraulic performance ( $\eta_{\text{combined}}$ ).....	44
Summary .....	46
References.....	47
Chapter 5 Conclusions and Future Recommendations .....	48
5.1. Conclusions .....	48
5.2. Future Recommendations.....	49
Appendix I: Research Article.....	51

## List of Figures

Fig. 1.1 (a) Graphical representation of global Renewable Energy Generation in the world (2000–2020) (b) Graphical representation of global Renewable Energy Consumption in the world (2000–2019) [8] .....	1
Fig. 1.2 Installed Global Renewable Energy by Technology [9].....	2
Fig. 1.3 Components of a solar air heater .....	3
Fig. 1.4 Classifications of solar air heaters [13] .....	4
Fig. 2.1 Rib Roughend Absorber Surface [7] .....	12
Fig. 2.2 SAH with Impingement Configuration [24].....	15
Fig. 2.3 SAH having both Air Impingement Configuration and Artificial Roughness [26].....	16
Fig. 3.1 Completely enclosed geometry .....	24
Fig. 3.2 Exploded view of the geometry .....	24
Fig. 3.3 Rectangular sectioned V-ribs on the test section of the absorber.....	25
Fig. 3.4 Air jet holes on the test section of the impingement plate.....	25
Fig. 3.5 Extracted fluid domain .....	26
Fig. 3.6 Detailed view of the meshed domain .....	27
Fig. 4.1 (a) Nu validation against Dittus Boelter equation (b) ff validation against Blasius equation .....	34
Fig. 4.2 (a) Nu validation against impingement correlation (b) ff validation against impingement correlation .....	35
Fig. 4.3 Temperature distribution at $Re = 12000$ on test section of (a) smooth absorber (b) absorber with rectangular sectioned V-ribs.....	36
Fig. 4.4 Change in Nu against Re as a function of (a) $e/D_h$ (b) $P/D_h$ and (c) $\alpha$ .....	38
Fig. 4.5 Contours of Turbulent kinetic energy at $e/D_h = 0.020$ , $P/D_h = 0.528$ , $\alpha = 60^\circ$ for Re (a) 3000 (b) 6000 (c) 12000 (d) 15000 (e) 18000.....	39
Fig. 4.6 Comparison of Nu with literature at various values of Re .....	40
Fig. 4.7 Contours of Turbulent kinetic energy at $Re = 9000$ at $e/D_h = 0.020$ , $P/D_h = 0.528$ , $\alpha = 60^\circ$ (a) Test section (b) enlarged view.....	41
Fig. 4.8 Change in ff against Re as a function of (a) $e/D_h$ (b) $P/D_h$ and (c) $\alpha$ .....	43
Fig. 4.9 Comparison of ff with literature at various values of Re.....	44
Fig. 4.10 Change in $\eta_{combined}$ against Re as a function of (a) $e/D_h$ (b) $P/D_h$ and (c) $\alpha$ .....	45



## **List of Tables**

Table 3.1 Range of roughness, impingement, and flow parameters .....	26
Table 3.2 Grid independency test .....	28
Table 3.3 Thermophysical properties.....	29
Table 3.4 Boundary conditions .....	30

## **List of Publications**

1. Muhammad Haroon Iqbal, Naveed Ahmed, Majid Ali, Mumtaz A Qaisrani, Mariam Mahmood, Adeel Waqas, Muhammad Bilal Sajid, “Numerical analysis of a solar air heater having rectangular sectioned V-ribs as artificial roughness integrated with impingement cooling configuration,” *Sustainable Energy Technologies and Assessment*, 2022. (Under review)

## List of Nomenclature

$a_k$	inverse effective Prandtl number for $k$
$a_\epsilon$	inverse effective Prandtl number for $\epsilon$
$C_p$	specific heat of air, J/kg k
$D_h$	hydraulic diameter of rectangular air duct, m
$h$	heat transfer coefficient, W/m <sup>2</sup> k
$k$	thermal conductivity of air, W/m k
$K$	turbulence kinetic energy, m <sup>2</sup> /s <sup>2</sup>
$L$	length of the test section, m
$P$	roughness pitch, m
$(\Delta P)_d$	pressure drop across the test section, Pa
$S_k$	user-defined source terms for $k$
$S_\epsilon$	user-defined source terms for $\epsilon$
$u$	airflow velocity in the x direction, m/s
$V_a$	velocity of the ambient air entering the duct, m/s
$v$	airflow velocity in the y direction, m/s
$w$	airflow velocity in the z direction, m/s

### Dimensionless parameters

$D_j/D_h$	relative jet diameter
$e/D_h$	relative roughness height
$ff$	friction factor
$ff_{combined}$	friction factor for air impingement onto an absorber having roughness
$ff_{imp}$	friction factor for air impingement onto a smooth absorber
$ff_{smooth}$	friction factor for smooth air duct
$Nu$	Nusselt number
$Nu_{combined}$	Nusselt number for air impingement onto an absorber having roughness
$Nu_{imp}$	Nusselt number for air impingement onto a smooth absorber
$Nu_{smooth}$	Nusselt Number for smooth air duct
$P/D_h$	relative roughness pitch
$Re$	Reynolds number
$X_j/D_h$	Relative stream-wise pitch

$Y_j/D_h$  Relative span-wise pitch

**Greek symbols**

$\alpha$  angle of attack, degree

$\eta_{\text{combined}}$  thermohydraulic performance

$\mu$  viscosity, kg/m-s

$\rho$  density, kg/m<sup>3</sup>

$\varepsilon$  dissipation rate, m<sup>2</sup>/s<sup>3</sup>

# Chapter 1

## Introduction

### 1.1. Background

Fastly growing populations and immense industrial growth have caused an imbalance between energy demand and supply. Despite their major health and environmental disadvantages [1,2], fossil fuels are still the main source of energy. Combustion of fossil fuels results in the emission of greenhouse gases. Given the recent growth in industry, the emission of greenhouse gases is expected to rise exponentially. It is estimated that if dependence on fossil fuels does not change then there will be severe changes in climate leading to severe weather change and health problems [3]. Such consequences of continuously utilizing fossil fuels can put the mere existence of human beings in jeopardy [4,5]. In an effort to reduce greenhouse gas emissions and dependence on depleting fossil fuels, many countries have been focusing on promoting renewable energy technologies. They are leaning towards implementing policies that can lead them toward carbon neutralization and ensure sustainable yet green industrial growth [6].

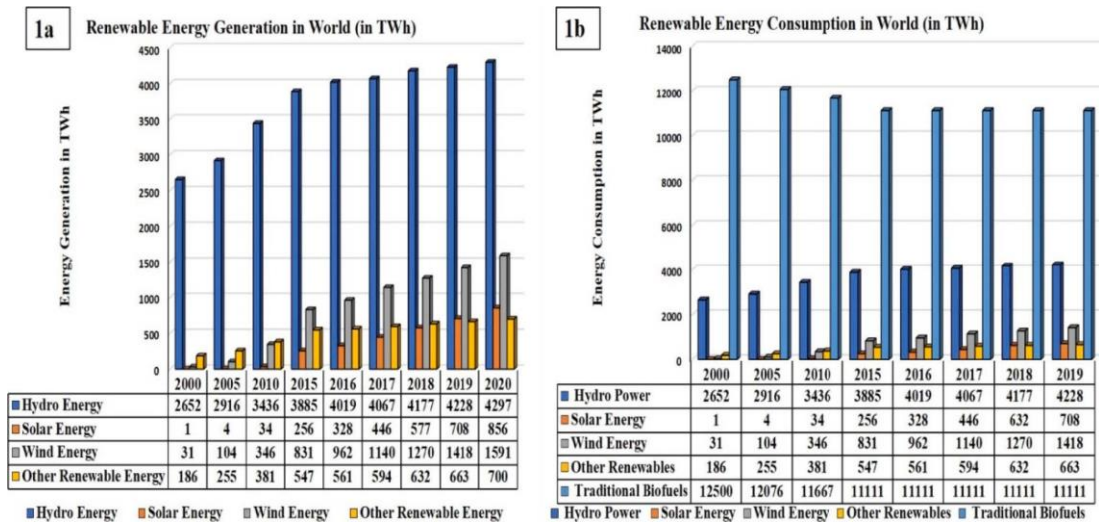


Fig. 1.1 (a) Graphical representation of global Renewable Energy Generation in the world (2000–2020) (b) Graphical representation of global Renewable Energy Consumption in the world (2000–2019) [8]

Renewable energy resources not only mitigate the adverse effects of utilizing fossil fuels but also help in maintaining economic growth [7]. Therefore, the world's current energy mix is going through an immense transition from conventional resources such as coal, gas, oil and petroleum to renewable energy resources such as hydro, solar, wind and others. Fig. 1.1 provides information about the yearly generated renewable energy and its consumption [8].

Renewable energy in its various forms, especially solar energy, is playing a key role to bridge the gap of increased energy demand for sustainable industrial growth [9]. It is estimated that solar energy that reaches our atmosphere in the form of radiation is 200 times greater than what humans consume in the form of commercial power. This fact alone speaks volumes to the potential of solar energy to meet the ever-growing energy demands. Solar energy can be transformed into either electrical energy or thermal energy. Devices such as Photovoltaic (PV) cells convert solar light to electrical energy using semi-conducting material while Concentrated Solar Power (CSP) plants use solar energy to convert it to thermal energy or high-temperature heat using concentrated mirrors which in turn is transformed to electrical energy using heat engines [8].

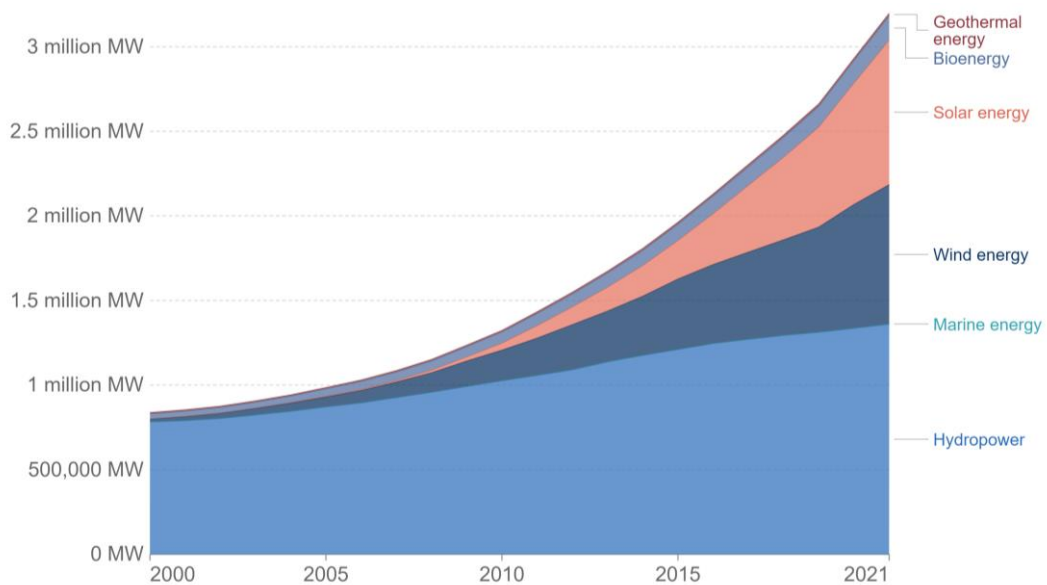


Fig. 1.2 Installed Global Renewable Energy by Technology [9]

Solar energy is also being put to good use for heating purposes using solar water heating systems [10] and solar desalination systems [11].

Moreover, solar energy through the introduction of solar air heaters can be utilized for space heating in buildings, crop drying and many industrial processes [12].

## 1.2. Principle

A conventional solar air heater consists of the following components.

- Glass cover
- Absorber plate
- Inlet and outlet sections
- Back and side plates – insulation

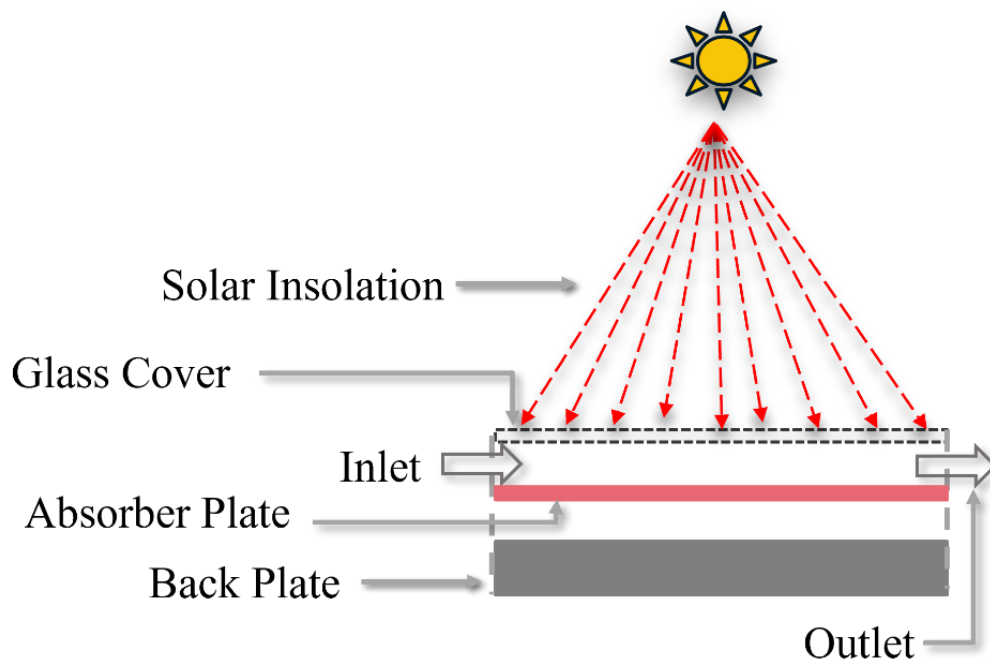


Fig. 1.3 Components of a solar air heater

The basic configuration of a solar air heater along with its components is given in Fig. 1.3. Solar air heaters, in their fundamental configurations, are heat exchangers. Glass cover receives the radiation from the sun and transmits it into the duct. The absorber plate gets heated by absorbing radiation from the sun and as air enters the duct from the inlet section, it comes in contact with the heated absorber. The convection heat transfer takes place in the duct where the absorber plate is cooled by the ambient air. Consequently, air attains a higher temperature, and this heated air is then collected from the outlet section. The side and bottom plates of a solar air heater constitute a duct and are typically made of plywood material. In addition, the bottom and side plates are covered with glass wool or mineral wool to avoid any heat losses during the

process. The absorber plate is usually painted black in order to increase radiation absorption.

Solar air heaters are classified based on various categories as flow patterns, applications, hybriding, collector (absorber) materials, glass covers, flow types, and collector (absorber) surface type [13]. These types are provided in Fig. 1.4.

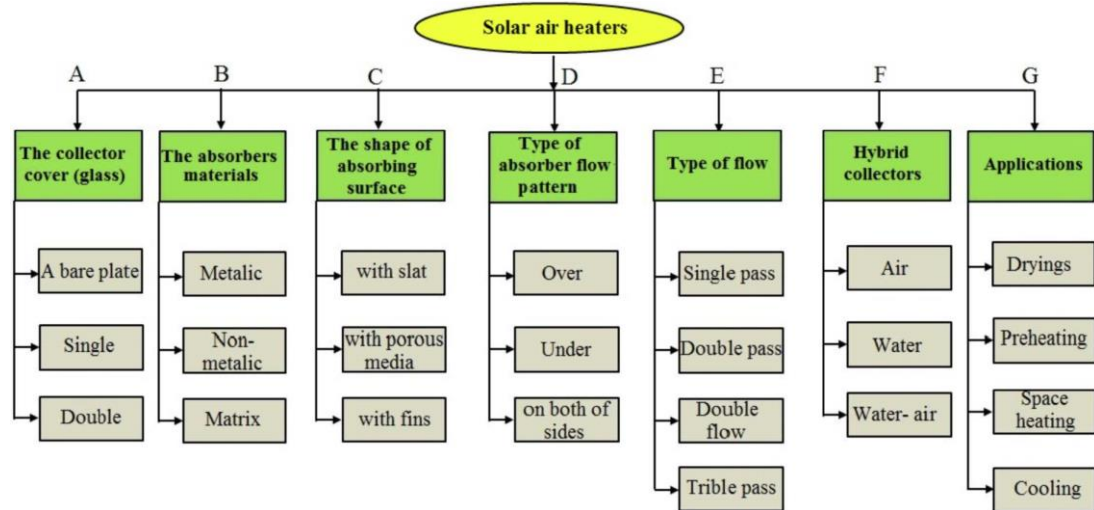


Fig. 1.4 Classifications of solar air heaters [13]

### 1.3. Problem Statement

Solar air heaters, in their fundamental configurations, are heat exchangers and their performance is characterized by the heat transfer interaction between the absorber surface and air. In a typical single-duct flat plate solar air heater, the heat transfer coefficient of air is considerably low owing to a sublayer formation over the heated surface. This causes the surface temperature of the heated surface to be considerably higher. Consequently, the heat losses to the ambient are significant and, therefore, efficiencies of solar air heaters are inherently low [14].

To augment the thermal performance, many researchers have conducted studies on solar air heaters which have mainly focused on either introducing artificial roughness on absorber plates like dimples, ribs, protrusions and wires in different shapes, orientations, and varying distances or making changes in the airflow passages with respect to the absorber.

Evidently, the literature suggests that different types of configurations especially V-ribs, air impingement and combined technique of ribs with air impingement have been



employed by researchers. However, a rectangular solar air channel comprising impinging air jets and rectangular sectioned V-ribs as artificial roughness has not been investigated to this date. Furthermore, a number of past studies [15–21] imply that the numerical technique has proven to be inexpensive, less time-consuming and an accurate way of computing the thermal and hydraulic characteristics in SAHs.

## **1.4. Research Objectives**

The goals of this study are.

- To augment the convection heat transfer rate between air and the absorber in a solar air heater.
- To numerically investigate the combined cooling effect of air impingement and an absorber having rectangular sectioned V-ribs as artificial roughness on thermal characteristics of solar air heater using a validated numerical model.
- To numerically investigate the combined cooling effect of air impingement and an absorber having rectangular sectioned V-ribs as artificial roughness on hydraulic characteristics of solar air heater using a validated numerical model.

## **1.5. Scope and Limitations**

### **1.5.1. Scope**

This study numerically models a solar air heater having the combined configuration of air impingement and an absorber having rectangular sectioned V-ribs as artificial roughness using a validated numerical model. The study addresses the low efficiency of the solar air heater by introducing novel cooling configurations. The effect of the combined configuration of air impingement and an absorber having rectangular sectioned V-ribs as artificial roughness on heat transfer and flow characteristics are discussed extensively, followed by the thermo-hydraulic performance of the proposed design.

### **1.5.2. Limitations**

The study uses numerical modeling to perform the analysis; therefore, assumptions are made to model the problem. Due to limited computational sources, RANS simulations are performed using turbulence modeling, which has good accuracy and is most widely used in today's world. The study is performed considering the heat flux of  $1000 \text{ W/m}^2$  on the top surface of the absorber.

## **1.6. Organization of thesis**

This thesis is divided into five chapters namely Introduction, Literature Review, Methodology, Results and Discussions, and Conclusions and Future Recommendations. Chapter 1 introduces the topic of this thesis. It provides information on how the use of fossil fuels is affecting the climate and emphasizes the use of renewable energy resources, especially solar energy. Then the chapter introduces the use of solar air heaters, its basic principle, scope, and goal of research. Chapter 2 provides a thorough analysis of literature and discusses different types of heat transfer augmentation techniques. Chapter 3 elaborates the methodology to complete this research. It provides information about computational domain, mesh generation, selection of a turbulence mode, grid independence test, boundary conditions and solution methods. Validation of the proposed numerical model is discussed in Chapter 4. In addition, heat transfer and flow characteristics of proposed model are discussed along with thermo-hydraulic performance. Chapter 5 sums up the objectives, methodology and results obtained and provides information on the possible future prospects of this study.

## **Summary**

In this chapter, the need for a transition from conventional energy resources to renewable energy resources is discussed. The conversion of solar energy to usable energy through different devices is elaborated. Moreover, the working principle of a solar air heater, its components and its classifications are presented in detail. The chapter also provides information on the scope and limitations of the study. Additionally, the research objectives are also presented in this chapter.

## References

- [1] X. Yang, J. Pang, F. Teng, R. Gong, and C. Springer, “The environmental co-benefit and economic impact of China’s low-carbon pathways: Evidence from linking bottom-up and top-down models,” *Renew. Sustain. Energy Rev.*, vol. 136, no. September 2020, p. 110438, 2021, doi: 10.1016/j.rser.2020.110438.
- [2] J. Curtin, C. McInerney, B. Ó Gallachóir, C. Hickey, P. Deane, and P. Deeney, “Quantifying stranding risk for fossil fuel assets and implications for renewable energy investment: A review of the literature,” *Renew. Sustain. Energy Rev.*, vol. 116, no. January, p. 109402, 2019, doi: 10.1016/j.rser.2019.109402.
- [3] A. G. Olabi et al., “Assessment of the pre-combustion carbon capture contribution into sustainable development goals SDGs using novel indicators,” *Renew. Sustain. Energy Rev.*, vol. 153, no. June 2021, p. 111710, 2022, doi: 10.1016/j.rser.2021.111710.
- [4] L. Gustavsson, T. Nguyen, R. Sathre, and U. Y. A. Tettey, “Climate effects of forestry and substitution of concrete buildings and fossil energy,” *Renew. Sustain. Energy Rev.*, vol. 136, no. August 2020, p. 110435, 2021, doi: 10.1016/j.rser.2020.110435.
- [5] X. He et al., “Well-to-wheels emissions, costs, and feedstock potentials for light-duty hydrogen fuel cell vehicles in China in 2017 and 2030,” *Renew. Sustain. Energy Rev.*, vol. 137, no. January 2020, 2021, doi: 10.1016/j.rser.2020.110477.
- [6] R. Madurai Elavarasan, S. Afridhis, R. R. Vijayaraghavan, U. Subramaniam, and M. Nurunnabi, “SWOT analysis: A framework for comprehensive evaluation of drivers and barriers for renewable energy development in significant countries,” *Energy Reports*, vol. 6, pp. 1838–1864, 2020, doi: 10.1016/j.egy.2020.07.007.
- [7] J. Wang, S. Zhang, and Q. Zhang, “The relationship of renewable energy consumption to financial development and economic growth in China,” *Renew. Energy*, vol. 170, pp. 897–904, 2021, doi: 10.1016/j.renene.2021.02.038.
- [8] C. M. S. Kumar et al., “Solar energy: A promising renewable source for meeting

- energy demand in Indian agriculture applications,” *Sustain. Energy Technol. Assessments*, vol. 55, no. November 2022, 2023, doi: 10.1016/j.seta.2022.102905.
- [9] M. K. Abdelrazik, S. E. Abdelaziz, M. F. Hassan, and T. M. Hatem, “Climate action: Prospects of solar energy in Africa,” *Energy Reports*, vol. 8, pp. 11363–11377, 2022, doi: 10.1016/j.egyr.2022.08.252.
- [10] A. Araújo, A. C. Ferreira, C. Oliveira, R. Silva, and V. Pereira, “Optimization of collector area and storage volume in domestic solar water heating systems with on–off control—A thermal energy analysis based on a pre-specified system performance,” *Appl. Therm. Eng.*, vol. 219, no. PD, p. 119630, 2023, doi: 10.1016/j.applthermaleng.2022.119630.
- [11] S. Shoeibi, H. Kargarsharifabad, S. A. A. Mirjalily, and T. Muhammad, “Solar district heating with solar desalination using energy storage material for domestic hot water and drinking water – Environmental and economic analysis,” *Sustain. Energy Technol. Assessments*, vol. 49, no. October 2021, p. 101713, 2022, doi: 10.1016/j.seta.2021.101713.
- [12] P. R. Olivkar, V. P. Katekar, S. S. Deshmukh, and S. V. Palatkar, “Effect of sensible heat storage materials on the thermal performance of solar air heaters: State-of-the-art review,” *Renew. Sustain. Energy Rev.*, vol. 157, no. September 2021, p. 112085, 2022, doi: 10.1016/j.rser.2022.112085.
- [13] H. K. Ghritlahre, M. Verma, J. S. Parihar, D. S. Mondloe, and S. Agrawal, “A detailed review of various types of solar air heaters performance,” *Sol. Energy*, vol. 237, no. April, pp. 173–195, 2022, doi: 10.1016/j.solener.2022.03.042.
- [14] V. Goel et al., “A comprehensive study on the progressive development and applications of solar air heaters,” *Sol. Energy*, vol. 229, no. February, pp. 112–147, 2021, doi: 10.1016/j.solener.2021.07.040.
- [15] A. S. Yadav, V. Shrivastava, A. Sharma, and M. K. Dwivedi, “Numerical simulation and CFD-based correlations for artificially roughened solar air heater,” *Mater. Today Proc.*, vol. 47, pp. 2685–2693, 2021, doi: 10.1016/j.matpr.2021.02.759.
- [16] T. Alam and M. H. Kim, “Heat transfer enhancement in solar air heater duct

- with conical protrusion roughness ribs,” *Appl. Therm. Eng.*, vol. 126, pp. 458–469, 2017, doi: 10.1016/j.applthermaleng.2017.07.181.
- [17] D. S. Thakur, M. K. Khan, and M. Pathak, “Solar air heater with hyperbolic ribs: 3D simulation with experimental validation,” *Renew. Energy*, vol. 113, pp. 357–368, 2017, doi: 10.1016/j.renene.2017.05.096.
- [18] A. S. Hussien and B. A. Zeru, “Design , Optimization and CFD Simulation of Solar Air Heater with Jet Impingement on V-Corrugated Plate,” *Int. Res. J. Eng. Technol.*, vol. 7, no. 05, pp. 1805–1813, 2020.
- [19] A. S. Yadav, A. Agrawal, A. Sharma, and A. Gupta, “Revisiting the effect of ribs on performance of solar air heater using CFD approach,” *Mater. Today Proc.*, vol. 63, pp. 240–252, 2022, doi: 10.1016/j.matpr.2022.02.549.
- [20] H. Singh, H. Singh, and C. Kishore, “CFD numerical investigation of Heat transfer characteristics of Y- shaped solar air heater,” *Mater. Today Proc.*, vol. 52, pp. 2003–2013, 2022, doi: 10.1016/j.matpr.2021.12.007.
- [21] H. Singh, H. Singh, R. Bahuguna, and C. Kishore, “CFD analysis of heat transfer characteristics of rectangular solar air heater with kite shaped roughness,” *Mater. Today Proc.*, vol. 52, pp. 2014–2025, 2022, doi: 10.1016/j.matpr.2021.12.008.

# Chapter 2

## Literature Review

Due to global climate change, the world's current energy mix is going through an immense transition. Renewable energy in its various forms, especially solar energy, is playing a key role to bridge the gap of increased energy demand for sustainable industrial growth [1]. Solar energy through the introduction of SAHs can be utilized for space heating in buildings, crop drying and many industrial processes [2]. SAHs, in their fundamental configurations, are heat exchangers and their performance is characterized by the heat transfer interaction between the absorber surface and air. In a typical single-duct flat plate SAH, the heat transfer coefficient of air is considerably low. This causes the surface temperature of the heated surface to be considerably higher. Consequently, the heat losses to the ambient are significant and, therefore, efficiencies of SAHs are inherently low [3].

### 2.1. Augmentation Techniques

To augment the thermal performance, many researchers have conducted studies on SAHs which have mainly focused on either introducing artificial roughness on absorber plates like dimples, ribs, protrusions and wires in different shapes, orientations, and varying distances or making changes in the airflow passages with respect to the absorber. Basically, one the following techniques or a combination of these techniques are used by the researchers.

- Use of Artificial roughness
- Use of Air impingement
- Using double pass, triple pass method

Considering the scope of this study, literature study on the technique of using artificial roughness and air impingement to enhance thermal performance of solar air heaters is completed and provided in the following subsections.

### 2.2. Artificial Roughness

The technique of using artificial roughness such as ribs on the absorber surface in SAHs is an effective method of augmenting the low thermal performance. These

artificial roughness act as turbulators in the path of air and can help break the viscous boundary layer [4].

Prasad and Saini [5] utilized protrusion wires having small diameters in a fully developed turbulent flow SAH system and observed that the wires effectively double the heat transfer rate. In addition, he found that this increase is accompanied by an increase in pressure drop. In turn, the friction factor of the solar air heater was increased four folds as compared to a flat plate solar air heater.

Gupta et al. [6] examined the optimum design parameters of a SAH system with non-transverse ribs. They evaluated that as compared to a smooth; a roughened SAH system is thermally more efficient. Moreover, the observations included that roughened SAHs performed thermo-hydraulically better at lower flowrate, but the smooth SAH are more thermo-hydraulically at higher Reynolds number.

Lau et al. [7] conducted experiments on a square channel roughened modeled as the internal cooling channels of a gas turbine with two opposite sides having V-shaped ribs to find the optimum angles of attack. They carried out experiments using  $45^\circ$ ,  $60^\circ$ ,  $90^\circ$ ,  $120^\circ$ , and  $135^\circ$  as angles of attack of the V-shaped rib configurations. The results showed that angle of attack of  $60^\circ$  gains highest heat transfer per increase in pressure drop.

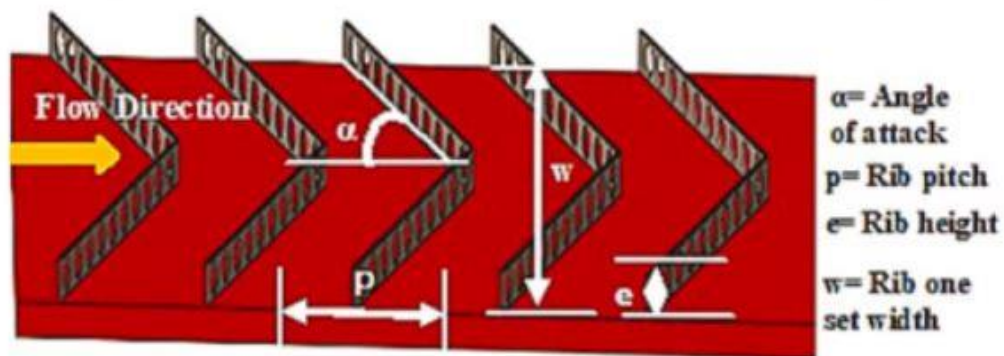


Fig. 2.1 Rib Roughend Absorber Surface [7]

To augment the heat transfer coefficient, Karwa et al. [8] used chamfered rib roughness having various roughness height, pitch and chamfer angles on the heated surface. They conducted experiments in the Reynolds number range of 3000 to 20,000 by heating the roughened wall while keeping the other three walls insulated. The study concluded that in comparison to the smooth duct, the roughened wall gains about two times



increase in the Stanton number while increase in pressure drop was observed to be three times as compared to a smooth wall. In addition, using a combined dimensionless number, they also developed correlations to predict Nu and ff for varying geometrical configurations.

Another study [9] numerically estimated the performance of a SAH with tapered ribs using the CFD technique and predicted an optimum performance of 1.91. The researchers developed two zones (Aluminium as absorber zone and Air as fluid zone) to evaluate the performance of proposed SAH. They used Ansys ICEM CFD tool to generate a hybrid grid consisting of quadrilateral and triangular elements. Whereas the volume of the domain comprised of hexahedral and wedge elements. The study utilized RNG K- $\epsilon$  model with enhanced wall function and evaluated performance of the proposed SAH in Reynolds number range between 3800–18,000. The optimal parameters corresponding to the optimum performance are taper angle = 1.6°, P/e = 10.7 at Re = 12,000.

Another numerical study by Yadav et al. [10] used a similar approach and investigated the performance enhancement of a roughened SAH. The researchers designed the absorber plate of ribbed solar heater with combination of circular and semi-circular ribs. They utilized ANSYS FLUENT CFD code to numerically investigate the ribbed square channel in 2D. The results showed that circular and semi-circular ribs having a lower pitch of 10 mm exhibit relatively higher heat transfer rate in contrast to higher pitch values. While Chandra et al. [11] compared the heat transfer enhancement and friction factor of ribs having cross sections of circular, semicircular, square and triangular in a square solar air channel. The results indicated square ribs achieve more heat transfer in comparison to other cross sections.

Several studies have focused on utilizing the advantages of secondary flow and lower negative pressure zone of V-shaped ribs or simply v-ribs as artificial roughness. Caliskan and Baskaya [12] discussed heat transfer measurements on a surface having rib roughness of V-shape and convergent-divergent configurations using infrared thermal images. The experiments consisted of blower, frequency controller, plenum, jet plate, Dantec 2-D LDA system, 3-D traverse system, an infrared thermal imaging system, and LabVIEW software system. Experimental results showed that V-shaped ribs produce more heat transfer as compared to convergent-divergent-shaped ribs.

A study performed by Momin et al. [13], effectively utilized V-shaped ribs to enhance the thermal performance of SAH. V-shaped rib roughness was provided on the underside of the absorber surface. The experiments considered the flow rate in the range of Re from 2500-18000, relative roughness height  $e/D_h$  from 0.02 to 0.034, angle of attack of flow from  $30^\circ$  to  $90^\circ$  while keeping the distance between consecutive ribs fixed to a value of 10. Experiments produced results with an overall increase of 2.30 in Nu and 2.83 times in ff at an angle of attack of  $60^\circ$  in contrast to a conventional SAH.

Hans et al. [14] used aluminum wires in the form of multiple v-ribs. The researchers used the lower surface of the absorber to attach multiple v-ribs. A rectangular duct made of wood was developed having an entry section of 0.525 m, test section of 1 m and exit section of 0.875 m. An auxiliary heater was used to provide the required heat flux of  $1000 \text{ W/m}^2$  onto the absorber surface. The results revealed that as compared to a flat plate SAH, they found significant improvements in Nu and ff of about 6 and 5 times respectively.

To understand the behavior of V-shaped rib roughness, Sharma and Bhargva [15] employed CFD analysis on a SAH. The study comprised multiple cases with  $e/D$  ranging from 0.02 to 0.04,  $P/e$  of 10 and  $\alpha$  in the range of  $30^\circ$  to  $90^\circ$ . The study utilized RNG k- $\epsilon$  turbulent model. A tetrahedral mesh structure was generated and numerical simulations on the proposed SAH were carried out in the range of Re from 4000 to 18000. It was discovered that the heat transfer varies directly as  $e/D$  increases, but the proposed system gives the best effective efficiency of 75% at  $e/D$  of 0.034.

### **2.3. Impingement Technique**

Moreover, the technique of making changes in the airflow passages with respect to the absorber through the introduction of jet impingement has also gained significant importance among many investigators lately. The applications of jet impingement can be found in solar thermal air receivers [16], internal cooling of turbine blades [17], and cooling of electronic devices [18].

Choudhury and Garg [19] were the first to utilize the cooling effect of jet impingement in SAHs. The researchers were able to attain a higher outlet air temperature and performance efficiency by  $15.5^\circ\text{C}$  and 26.5% respectively.

Later on, Chauhan and Thakur [20],[21] utilized air impingement cooling effect in SAH by varying relative jet diameter, relative streamwise pitch and relative spanwise pitch. The study utilized an auxiliary heater to maintain a heat flux of  $1000 \text{ W/m}^2$  on the absorber surface. They observed that as the interference between the two impinging air jets was of high importance. In addition, he found out that as this interference prior to impingement between the jets decreases, the boundary layer formed around the absorber surface becomes thinner. This phenomenon in turn favors the convection heat transfer between air and the heated absorber. Moreover, the study accomplished that utilizing impinging air jets, as compared to conventional flat plate heaters, encourages heat transfer, fluid flow and thermohydraulic performance characteristics by 2.67, 3.5 and 34.54 to 57.89% respectively.

Another study [22], analyzed the performance of impinging jets on a 1.6 mm thick steel plate. The study considered the parameters that could affect the heat transfer characteristics. The angle of the impinging jet air nozzle varied from  $0^\circ$  to  $90^\circ$ . The results showcased a maximum thermal improvement of 2.19 at a mass flow rate of 0.016 kg/s. Moreover, the results revealed that an angle of jet air nozzle of  $30^\circ$  produces the maximum heat transfer whereas the angle of  $0^\circ$  performs the lowest.

Moreover, Maithani et al. [23] used inclined perforated pipes for providing air onto the heated surface. The study determined that impinging jet pipe arrangement compliments  $Nu$  and  $ff$  by a factor of 3.25 and 8.45 respectively.

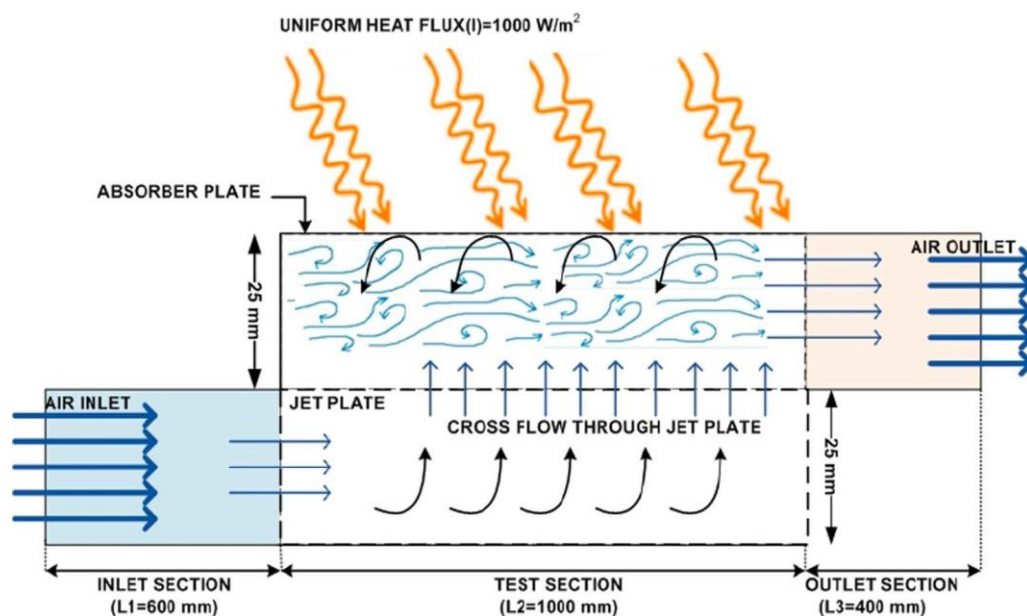


Fig. 2.2 SAH with Impingement Configuration [24]

After that, Yadav and Saini [24] carried out a numerical investigation on an impinging jet SAH system by varying jet height ratio in the range 0–0.433 and Reynolds number 3500–17,500 and found the thermal-hydraulic performance value to be 3.66 at jet diameter ratio = 0.065 and  $Re = 15,500$ . More recently, an analytical case study [25] used impingement configuration to attain a thermohydraulic performance of 68.12%.

## 2.4. Air Impingement with Artificial Roughness – A Combined Technique

The cooling effect of impinging jets and ribs impart flow separation and secondary flows to the airflow in SAH. Owing to these favorable factors, many scientists have also explored the idea of analyzing the combined effect of rib roughness as artificial roughness and air impingement using jets on thermal performance and fluid flow characteristics.

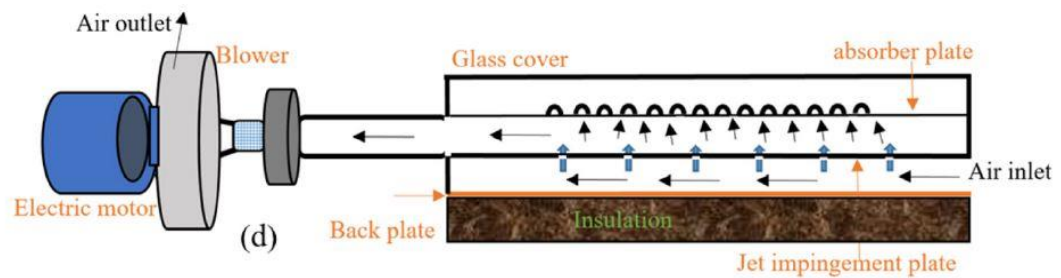


Fig. 2.3 SAH having both Air Impingement Configuration and Artificial Roughness [26]

Yan et al. [26] used a 5 mm thick jet plate to strike inline and staggered jet arrays of air onto a rib-roughened acrylic surface coated with a thermochromic liquid crystal (TLC). The image processing system depicted that inline and staggered jet arrangements at angles  $60^\circ$  and  $90^\circ$  show minute differences in heat transfer. Whereas ribs at an angle of  $45^\circ$  and the inline jet array illustrate better thermal results than the corresponding staggered jet arrangement. They attributed this effect to the advantageous development of vortices at the solid-fluid boundary.

Xing et al. [27] used a similar TLC approach for comparing the impingement cooling effect on a flat target plate with that of a micro rib-roughened target plate. They observed that the heat transfer effect of crossflow air impingement on micro-rib roughened target surface is 9.6% more than that for a flat target plate at  $Re = 35,000$ , and jet-to-plate spacing = 30 mm. Additionally, the research results were complemented by a detailed CFD analysis.

Nu and ff characteristics owing to the combined effect of having transverse ribs and impingement jet plate were examined by Moshery et al. [28]. Experiments and numerical investigations using transverse ribs were carried out on a 1.4 m long solar simulator with varying solar heat flux and mass flow rate. Consequently, they were able to attain a thermal efficiency of 78% at maximum values of heat flux and mass flow rate.

Kumar et al. [29] devised a solar simulator system having an impingement configuration coupled with arc protrusion rib roughness on the absorber surface. The proposed SAH configuration gave optimum thermohydraulic performance of 1.5 at an angle of arc protrusion of 60°.

## **2.5. Research Gap**

Evidently, the literature suggests that different types of configurations especially V-ribs, air impingement and combined technique of ribs with air impingement have been employed by researchers. However, a rectangular solar air channel comprising impinging air jets and rectangular sectioned V-ribs as artificial roughness has not been investigated to this date. Furthermore, a number of past studies [10,11],[27],[30–36] imply that the numerical technique has proven to be inexpensive, less time-consuming and an accurate way of computing the thermal and hydraulic characteristics in SAHs. Therefore, this study aims to numerically investigate the combined effect of air impingement and an absorber having rectangular sectioned V-ribs as artificial roughness on thermal and hydraulic characteristics in SAH using a validated numerical model.

## **Summary**

This chapter sheds light on several augmentation techniques for heat transfer and fluid flow characteristics such as artificial roughness, air impingement and artificial roughness with air impingement used by researchers in solar air heaters. Based on the reported results of these techniques presented in the literature review, the chapter draws the conclusion that combined cooling of a rectangular solar air channel comprising impinging air jets and rectangular sectioned V-ribs as artificial roughness has not been investigated to this date. Therefore, this study aims to numerically investigate the combined effect of air impingement and an absorber having rectangular sectioned V-ribs as artificial roughness on thermal and hydraulic characteristics in SAH using a validated numerical model.

## References

- [1] M. K. Abdelrazik, S. E. Abdelaziz, M. F. Hassan, and T. M. Hatem, “Climate action: Prospects of solar energy in Africa,” *Energy Reports*, vol. 8, pp. 11363–11377, 2022, doi: 10.1016/j.egy.2022.08.252.
- [2] P. R. Olivkar, V. P. Katekar, S. S. Deshmukh, and S. V. Palatkar, “Effect of sensible heat storage materials on the thermal performance of solar air heaters: State-of-the-art review,” *Renew. Sustain. Energy Rev.*, vol. 157, no. September 2021, p. 112085, 2022, doi: 10.1016/j.rser.2022.112085.
- [3] V. Goel et al., “A comprehensive study on the progressive development and applications of solar air heaters,” *Sol. Energy*, vol. 229, no. February, pp. 112–147, 2021, doi: 10.1016/j.solener.2021.07.040.
- [4] C. Gables, R. K. Shah, J. Wiley, and R. H. Pletcher, *SINGLE-PHASE CONVECTIVE*. .
- [5] Prasad. B.N and Saini. J.S, “Effect of artificial roughness on heat transfer and friction factor in a solar air heater,” *Sol. Energy*, vol. 41, no. 6, pp. 555–560, 1988.
- [6] D. Gupta, S. C. Solanki, and J. S. Saini, “Thermohydraeic performance of solar air heaters with roughened absorber plates,” *Sol. Energy*, vol. 61, no. 1, pp. 33–42, 1997, doi: 10.1016/S0038-092X(97)00005-4.
- [7] S. C. Lau, R. T. Kukreja, and R. D. Mcmillin, “Effects of V-shaped rib arrays on turbulent heat transfer and friction of fully developed flow in a square channel,” *Int. J. Heat Mass Transf.*, vol. 34, no. 7, pp. 1605–1616, 1991, doi: 10.1016/0017-9310(91)90140-A.
- [8] R. Karwa, S. C. Solanki, and J. S. Saini, “Heat transfer coefficient and friction factor correlations for the transitional flow regime in rib-roughened rectangular ducts,” *Int. J. Heat Mass Transf.*, vol. 42, no. 9, pp. 1597–1615, May 1999, doi: 10.1016/S0017-9310(98)00252-X.
- [9] A. D. Gupta and L. Varshney, “Performance prediction for solar air heater having rectangular sectioned tapered rib roughness using CFD,” *Therm. Sci. Eng. Prog.*, vol. 4, pp. 122–132, 2017, doi: 10.1016/j.tsep.2017.09.005.

- [10] A. S. Yadav, A. Mishra, K. Dwivedi, A. Agrawal, A. Galphat, and N. Sharma, "Investigation on performance enhancement due to rib roughened solar air heater," *Mater. Today Proc.*, vol. 63, pp. 726–730, 2022, doi: 10.1016/j.matpr.2022.05.071.
- [11] P. R. Chandra, M. L. Fontenot, and J. C. Han, "Effect of rib profiles on turbulent channel flow heat transfer," *J. Thermophys. Heat Transf.*, vol. 12, no. 1, pp. 116–118, 1998, doi: 10.2514/2.6312.
- [12] S. Caliskan and S. Baskaya, "Experimental investigation of impinging jet array heat transfer from a surface with V-shaped and convergent-divergent ribs," *Int. J. Therm. Sci.*, vol. 59, pp. 234–246, 2012, doi: 10.1016/j.ijthermalsci.2012.04.013.
- [13] A.-M. E. Momin, J. S. Saini, and S. C. Solanki, "Heat transfer and friction in solar air heater duct with V-shaped rib roughness on absorber plate," *Energy*, vol. 36, no. 7, pp. 4531–4541, 2002, doi: 10.1016/j.energy.2011.03.054.
- [14] V. S. Hans, R. P. Saini, and J. S. Saini, "Heat transfer and friction factor correlations for a solar air heater duct roughened artificially with multiple v-ribs," *Sol. Energy*, vol. 84, no. 6, pp. 898–911, 2010, doi: 10.1016/j.solener.2010.02.004.
- [15] M. Sharma and M. Bhargva, "CFD based performance analysis of solar air heater provided with artificial roughness in the form of V - Shaped ribs," *Mater. Today Proc.*, vol. 63, pp. 595–601, 2022, doi: 10.1016/j.matpr.2022.04.168.
- [16] M. Röger, R. Buck, and H. Müller-Steinhagen, "Numerical and experimental investigation of a multiple air jet cooling system for application in a solar thermal receiver," *J. Heat Transfer*, vol. 127, no. 8, pp. 863–876, 2005, doi: 10.1115/1.1928910.
- [17] J.-C. Han, "Recent Studies in Turbine Blade Cooling?," *Int. J. Rotating Mach.*, vol. 10, no. 6, pp. 443–457, 2004, doi: 10.1080/10236210490503978.
- [18] M. K. Sung and I. Mudawar, "Experimental and numerical investigation of single-phase heat transfer using a hybrid jet-impingement/micro-channel cooling scheme," *Int. J. Heat Mass Transf.*, vol. 49, no. 3–4, pp. 682–694, 2006, doi: 10.1016/j.ijheatmasstransfer.2005.08.021.



- [19] C. Choudhury, H. P. Garg, and H. Khas, "E V a L U a T I O N of a Jet Plate Solar Air Heater," *Sol. Energy*, vol. 46, no. 4, pp. 199–209, 1991.
- [20] R. Chauhan and N. S. Thakur, "Heat transfer and friction factor correlations for impinging jet solar air heater," *Exp. Therm. Fluid Sci.*, vol. 44, pp. 760–767, 2013, doi: 10.1016/j.expthermflusci.2012.09.019.
- [21] R. Chauhan and N. S. Thakur, "Investigation of the thermohydraulic performance of impinging jet solar air heater," *Energy*, vol. 68, pp. 255–261, 2014, doi: 10.1016/j.energy.2014.02.059.
- [22] T. Rajaseenivasan, S. Ravi Prasanth, M. Salamon Antony, and K. Srithar, "Experimental investigation on the performance of an impinging jet solar air heater," *Alexandria Eng. J.*, vol. 56, no. 1, pp. 63–69, 2017, doi: 10.1016/j.aej.2016.09.004.
- [23] R. Maithani, S. Sharma, and A. Kumar, "Thermo-hydraulic and exergy analysis of inclined impinging jets on absorber plate of solar air heater," *Renew. Energy*, vol. 179, pp. 84–95, 2021, doi: 10.1016/j.renene.2021.07.013.
- [24] S. Yadav and R. P. Saini, "Numerical investigation on the performance of a solar air heater using jet impingement with absorber plate," *Sol. Energy*, vol. 208, no. August, pp. 236–248, 2020, doi: 10.1016/j.solener.2020.07.088.
- [25] M. M. Matheswaran et al., "A case study on thermo-hydraulic performance of jet plate solar air heater using response surface methodology," *Case Stud. Therm. Eng.*, vol. 34, no. January, 2022, doi: 10.1016/j.csite.2022.101983.
- [26] W. M. Yan, H. C. Liu, C. Y. Soong, and W. J. Yang, "Experimental study of impinging heat transfer along rib-roughened walls by using transient liquid crystal technique," *Int. J. Heat Mass Transf.*, vol. 48, no. 12, pp. 2420–2428, 2005, doi: 10.1016/j.ijheatmasstransfer.2004.12.048.
- [27] Y. Xing, S. Spring, and B. Weigand, "Experimental and numerical investigation of impingement heat transfer on a flat and micro-rib roughened plate with different crossflow schemes," *Int. J. Therm. Sci.*, vol. 50, no. 7, pp. 1293–1307, 2011, doi: 10.1016/j.ijthermalsci.2010.11.008.
- [28] R. Moshery, T. Y. Chai, K. Sopian, A. Fudholi, and A. H. A. Al-Waeli,

- “Thermal performance of jet-impingement solar air heater with transverse ribs absorber plate,” *Sol. Energy*, vol. 214, no. December 2020, pp. 355–366, 2021, doi: 10.1016/j.solener.2020.11.059.
- [29] R. Kumar et al., “Heat transfer and friction factor correlations for an impinging air jets solar thermal collector with arc ribs on an absorber plate,” *Sustain. Energy Technol. Assessments*, vol. 47, no. May, p. 101523, 2021, doi: 10.1016/j.seta.2021.101523.
- [30] A. S. Yadav, A. Agrawal, A. Sharma, and A. Gupta, “Revisiting the effect of ribs on performance of solar air heater using CFD approach,” *Mater. Today Proc.*, vol. 63, pp. 240–252, 2022, doi: 10.1016/j.matpr.2022.02.549.
- [31] A. S. Hussien and B. A. Zeru, “Design , Optimization and CFD Simulation of Solar Air Heater with Jet Impingement on V-Corrugated Plate,” *Int. Res. J. Eng. Technol.*, vol. 7, no. 05, pp. 1805–1813, 2020.
- [32] D. S. Thakur, M. K. Khan, and M. Pathak, “Solar air heater with hyperbolic ribs: 3D simulation with experimental validation,” *Renew. Energy*, vol. 113, pp. 357–368, 2017, doi: 10.1016/j.renene.2017.05.096.
- [33] T. Alam and M. H. Kim, “Heat transfer enhancement in solar air heater duct with conical protrusion roughness ribs,” *Appl. Therm. Eng.*, vol. 126, pp. 458–469, 2017, doi: 10.1016/j.applthermaleng.2017.07.181.
- [34] A. S. Yadav, V. Shrivastava, A. Sharma, and M. K. Dwivedi, “Numerical simulation and CFD-based correlations for artificially roughened solar air heater,” *Mater. Today Proc.*, vol. 47, pp. 2685–2693, 2021, doi: 10.1016/j.matpr.2021.02.759.
- [35] H. Singh, H. Singh, R. Bahuguna, and C. Kishore, “CFD analysis of heat transfer characteristics of rectangular solar air heater with kite shaped roughness,” *Mater. Today Proc.*, vol. 52, pp. 2014–2025, 2022, doi: 10.1016/j.matpr.2021.12.008.
- [36] H. Singh, H. Singh, and C. Kishore, “CFD numerical investigation of Heat transfer characteristics of Y- shaped solar air heater,” *Mater. Today Proc.*, vol. 52, pp. 2003–2013, 2022, doi: 10.1016/j.matpr.2021.12.007.

# Chapter 3

## Methodology

This chapter gives an insight into the numerical modeling method and governing equations used to model the problem. Different approaches have been used in numerical modeling to solve the Navier Stokes problem. Reynolds averaged Navier Stokes (RANS) is computationally less expensive than Large Eddy Simulations (LES), while Direct Numerical Simulations (DNS) are the most expensive. DNS resolves the Navier Stokes directly. LES resolves large eddies and models the smaller eddies. While RANS model turbulence using turbulence models. RANS is computationally less expensive, widely being used, and yields good results while saving costs. RANS-based simulations are performed for this study.

In this chapter, the effect of utilizing rectangular sectioned V-ribs on the absorber surface in an impinging air jet SAH is evaluated using the finite volume method. 3D numerical analysis has been performed by varying roughness parameters  $e/D_h$ ,  $P/D_h$  and  $\alpha$  while keeping impingement parameters  $D_j/D_h$ ,  $X_j/D_h$ , and  $Y_j/D_h$  constant. The following subsections provide detailed information on numerical modeling from details of proposed design configurations to solution methods.

### 3.1. Model Creation

#### 3.1.1. Geometry Creation

The proposed geometry for the novel solar air heater is created using Solidworks and is presented in Fig. 3.1. The complete geometry mainly encompasses an absorber plate, an impingement plate and a back plate. The proposed duct with combined air impingement and V-ribs surface roughness consists of two ducts i.e., upper and lower duct. Both upper and lower rectangular ducts measure 2 x 0.3 x 0.025 m. The inlet section is 0.6 m long while the test and outlet sections are 1 m and 0.4 m long respectively. Lengths of the inlet and outlet sections have been calculated as per ASHRAE Standards [1].

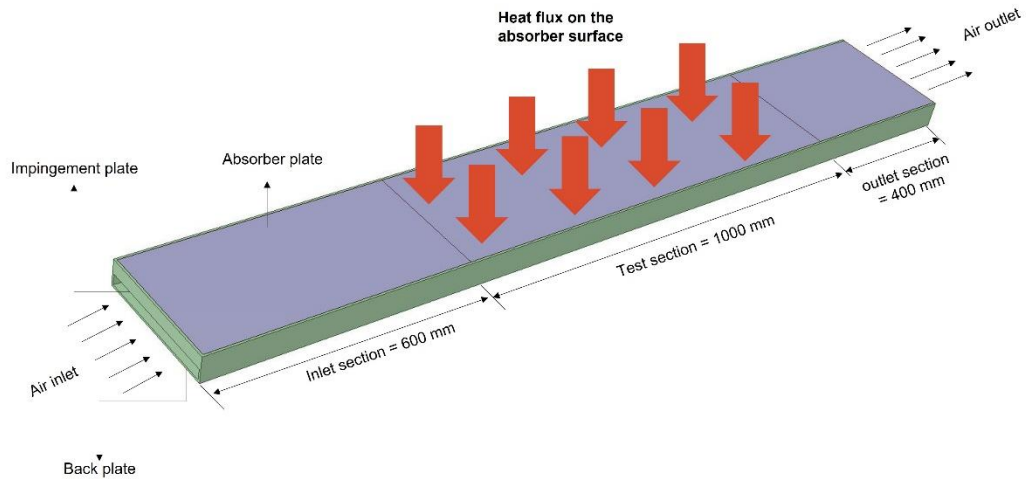


Fig. 3.1 Completely enclosed geometry

Fig. 3.2 provides information on the position of each component with respect to each other with an exploded view of the geometry.

Rectangular sectioned V-ribs are provided on the lower surface (only test section) of the absorber using a pattern function in Solidworks. The absorber is made of aluminum and is 2 mm thick, having a length and width the same as that of the duct. Rib roughness height, rib roughness pitch and angle of attack are normalized by the hydraulic diameter of the duct.

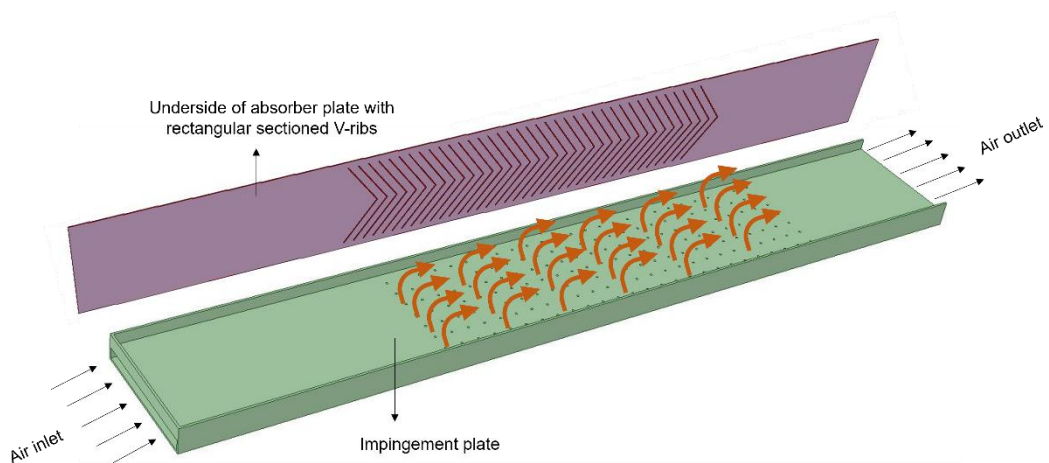


Fig. 3.2 Exploded view of the geometry

Twenty-seven (27) absorber plates are prepared for the numerical investigation by varying relative rib roughness height ( $e/D_h$ ), relative rib roughness pitch ( $P/D_h$ ) and

angle of attack ( $\alpha$ ) respectively. Fig. 3.3 shows a typical absorber plate having roughness parameters of  $e/D_h = 0.020$ ,  $P/D_h = 0.528$  and  $\alpha = 60^\circ$ .

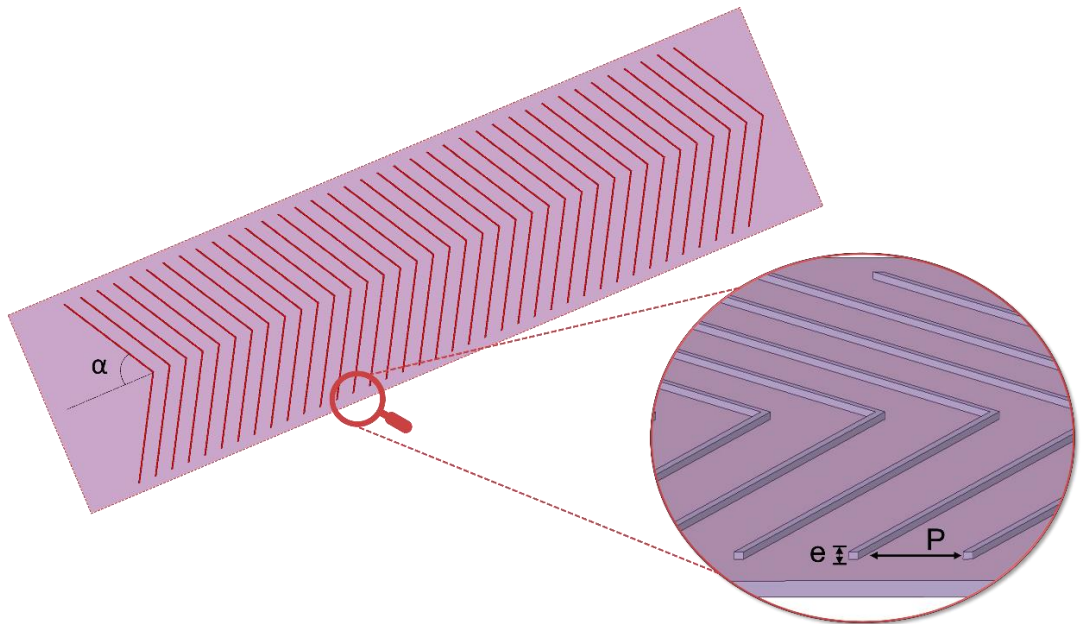


Fig. 3.3 Rectangular sectioned V-ribs on the test section of the absorber

An impingement plate 5 mm thick, having length and width the same as that of the duct is placed in between the back plate and absorber plate. As the name suggests, the impingement plate has holes in its test section and is made of wood.

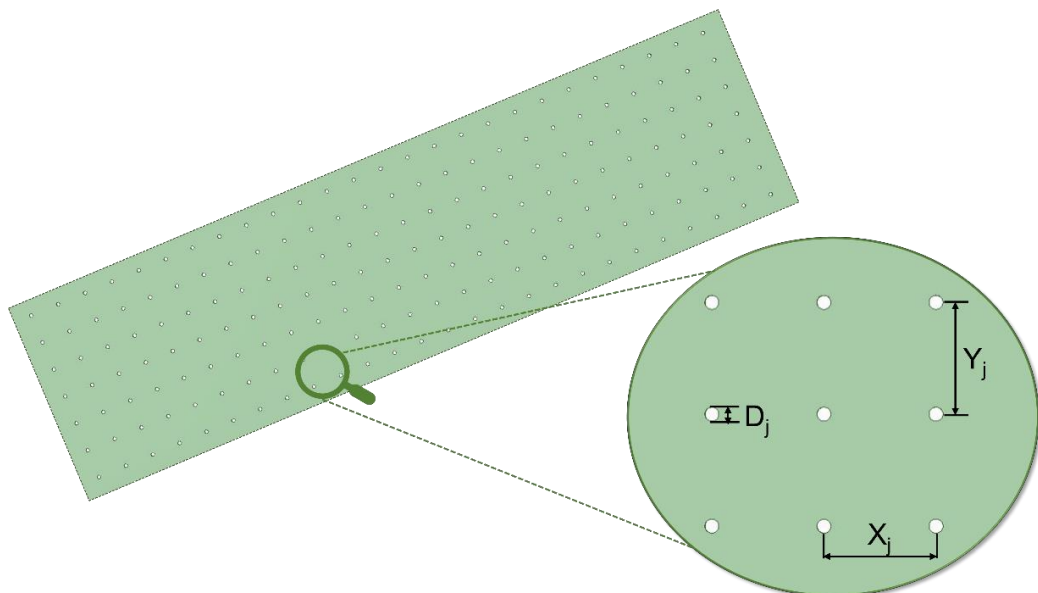


Fig. 3.4 Air jet holes on the test section of the impingement plate

Initially, a hole of 5 mm is created at a 0.6 m distance from the inlet using extrude cut function on Solidworks. This hole is repeated in the streamwise (X-axis) and spanwise

direction using the pattern function. Impingement parameters used to model the impingement plate are namely relative jet diameter ( $D_j/D_h$ ), relative streamwise pitch ( $X_j/D_h$ ), and relative spanwise pitch ( $Y_j/D_h$ ). These impingement parameters are kept fixed for all the numerical simulations. Fig. 3.4 shows an impingement plate having parameters of  $D_j/D_h = 0.108$ ,  $X_j/D_h = 0.867$  and  $Y_j/D_h = 0.867$ . Table 3.1 provides information on the range of geometrical and flow parameters used in this study.

**Table 3.1** Range of roughness, impingement, and flow parameters

S. No	Parameter	Range	Steps
1.	$e/D_h$	0.016–0.024	3
2.	$P/D_h$	0.264–0.792	3
3.	$\alpha$	$30^\circ$ – $75^\circ$	3
4.	$D_j/D_h$	0.108	fix
5.	$X_j/D_h$	0.867	fix
6.	$Y_j/D_h$	0.867	fix
7.	Re	3000–18000	6

### 3.1.2. Computational Domain and Mesh Generation

The modeled geometry shown in Fig. 3.1 is then imported to Ansys SpaceClaim and is checked for any repairs such as stitches, gaps, and missing faces. Using the volume extract function available in Ansys SpaceClaim, the fluid domain is extracted from the whole geometry and is shown in Fig. 3.5.

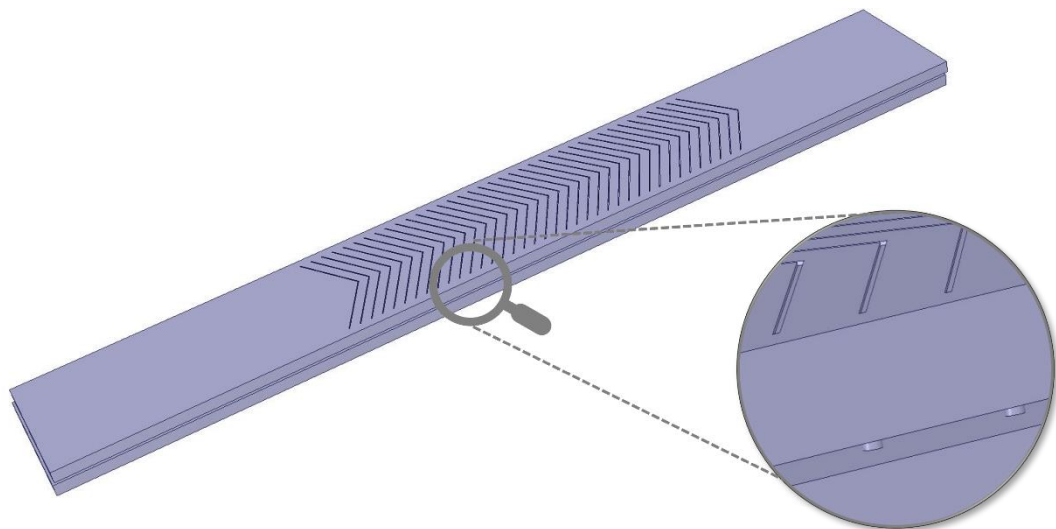


**Fig. 3.5** Extracted fluid domain

Considering the heat transfer and fluid flow interactions due to rectangular sectioned V-ribs on the lower surface of the absorber, the computational domain has been split into two zones.

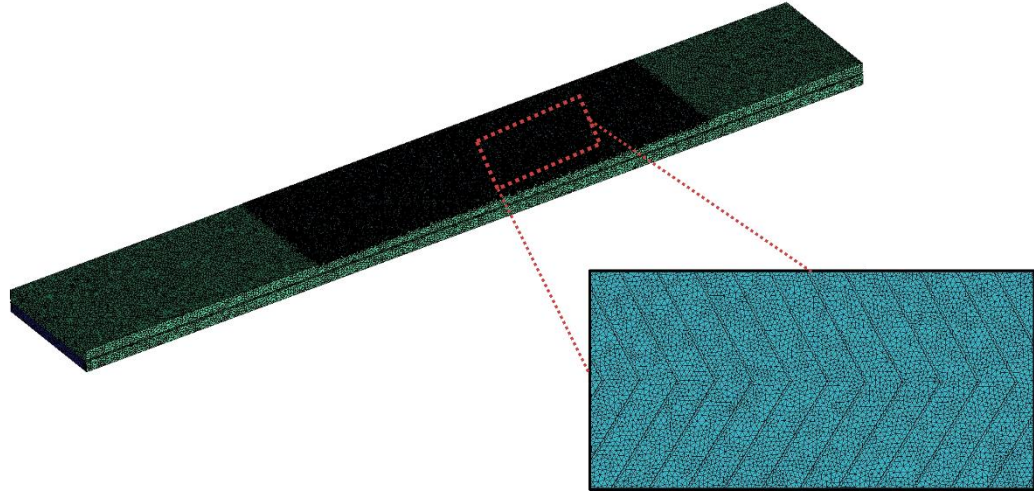


Fig. 3.6 Detailed view of the meshed domain

Air acts as the fluid zone as it enters the inlet section in the lower channel, passes through the air jets on the test section of the impingement plate, strikes the test section of the absorber having rectangular sectioned V-ribs in the upper channel, and leaves the duct from the outlet section. While the 2 mm thick absorber having rectangular sectioned V-ribs on its underside is regarded as the absorber zone.

The computational domain comprising of fluid and absorber zone is discretized into a grid of unstructured mesh using ICEM CFD and is shown in Fig. 3.6. To capture the boundary layer separation phenomenon and keep the  $Y^+$  value around unity, fine prism layers at the solid-fluid boundary have been created.

### 3.2. Grid Independence Study

Initially, a geometrical configuration of rectangular sectioned V-ribs having  $e/D_h = 0.020$ ,  $P/D_h = 0.528$  and  $\alpha = 60^\circ$  and impingement parameters of  $D_j/D_h = 0.108$ ,  $X_j/D_h = 0.867$  and  $Y_j/D_h = 0.867$  is selected to perform grid independence test for  $Re = 12000$ . Table 3.2 presents the effect of five consecutive denser grids on the percentage change in  $Nu$  and  $ff$ . It is evident that mesh size finer than  $18.96 \times 10^6$  cells result in an inconsiderable change in  $Nu$  and  $ff$ . Consequently, a grid size of  $18.96 \times 10^6$  elements has been considered for the numerical analysis.

Table 3.2 Grid independency test

S. No	No of elements	% Change in Nu	% Change in ff
1.	14.82×10 <sup>6</sup>	–	–
2.	16.43×10 <sup>6</sup>	3.7	4.1
3.	17.89×10 <sup>6</sup>	1.7	2.1
4.	18.96×10 <sup>6</sup>	0.72	0.98
5.	19.87×10 <sup>6</sup>	0.39	0.67

### 3.3. Turbulence Model

In order to minimize numerical errors, it is imperative to choose a suitable turbulence model. The criterion for an appropriate turbulence model is that it gives a solution nearly similar to experimental results by compromising between numerical effort and solution accuracy. A study [2] compares the four different models for smooth SAH. It concludes that the RNG k-ε model gives results identically similar in nature to that for smooth SAH as compared to other models. Additionally, studies [3,4] also used the RNG k-ε model to numerically investigate roughened SAHs. Therefore, for the present study, RNG k-ε model with enhanced wall function is utilized.

### 3.4. Governing Equations

The governing equations for mass, momentum, and energy conservation can be written in the following form [5].

Continuity Equation:

$$\frac{\partial \rho}{\partial t} + \frac{\partial(\rho u)}{\partial x} + \frac{\partial(\rho v)}{\partial y} + \frac{\partial(\rho w)}{\partial z} = 0 \quad (1)$$

Navier-Stokes equations

$$\rho \frac{\partial u}{\partial t} + \rho u \frac{\partial u}{\partial x} + \rho v \frac{\partial u}{\partial y} + \rho w \frac{\partial u}{\partial z} = -\frac{\partial \hat{p}}{\partial x} + \mu \left[ \frac{\partial^2 u}{\partial x^2} + \frac{\partial^2 u}{\partial y^2} + \frac{\partial^2 u}{\partial z^2} \right] \quad (2)$$

$$\rho \frac{\partial v}{\partial t} + \rho u \frac{\partial v}{\partial x} + \rho v \frac{\partial v}{\partial y} + \rho w \frac{\partial v}{\partial z} = -\frac{\partial \hat{p}}{\partial y} + \mu \left[ \frac{\partial^2 v}{\partial x^2} + \frac{\partial^2 v}{\partial y^2} + \frac{\partial^2 v}{\partial z^2} \right] \quad (3)$$



$$\rho \frac{\partial w}{\partial t} + \rho u \frac{\partial w}{\partial x} + \rho v \frac{\partial w}{\partial y} + \rho w \frac{\partial w}{\partial z} = -\frac{\partial \hat{p}}{\partial t} + \mu \left[ \frac{\partial^2 w}{\partial x^2} + \frac{\partial^2 w}{\partial y^2} + \frac{\partial^2 w}{\partial z^2} \right] \quad (4)$$

Transport equations for the Turbulence model can be written as

$$\frac{\partial}{\partial t}(\rho k) + \frac{\partial}{\partial x_j}(\rho k u_j) = \frac{\partial}{\partial x_j} \left[ a_k \mu_{eff} \frac{\partial k}{\partial x_j} \right] + G_k + G_b - \rho \varepsilon + Y_m + S_k \quad (5)$$

$$\frac{\partial}{\partial t}(\rho \varepsilon) + \frac{\partial}{\partial x_j}(\rho \varepsilon u_j) = \frac{\partial}{\partial x_j} \left[ a_\varepsilon \mu_{eff} \frac{\partial \varepsilon}{\partial x_j} \right] + C_{1\varepsilon} \frac{\varepsilon}{k} (G_k + C_{3\varepsilon} G_b) - C_{2\varepsilon} \rho \frac{\varepsilon^2}{k} - R_\varepsilon + S_\varepsilon \quad (6)$$

$G_k$  represents the generation of TKE owing to mean velocity gradients whereas  $G_b$  is the generation of TKE because of buoyancy. Furthermore,  $C_{1\varepsilon}$ ,  $C_{2\varepsilon}$  and  $C_{3\varepsilon}$  are constants and correspond to a value of 1.42, 1.68 and 1.3 respectively. Moreover,  $Re$  of the fluid,  $Nu$  and  $ff$  are determined by using the following equations respectively from the literature [6].

$$Re = \frac{\rho_a V_a D_h}{\mu} \quad (7)$$

Whereas  $V_a$  represents the velocity of the ambient air entering the lower channel.

$$Nu = \frac{h D_h}{k} \quad (8)$$

$$ff = \frac{2(\Delta P)_d D_h}{4\rho_a L V_a^2} \quad (9)$$

### 3.5. Boundary conditions and solution methods

A 3-D computational domain consisting of two zones, air and absorber, has been considered for numerical analysis. Table 3.3 presents the thermophysical properties of air and aluminum absorber.

Table 3.3 Thermophysical properties

	Density, $\rho$ (kg/m <sup>3</sup> )	Viscosity, $\mu$ (kg/m-s)	Thermal conductivity, $k$ (W/m-K)	Specific Heat, $C_p$ (J/kg-K)
Air	1.225	$1.7894 \times 10^{-5}$	0.0242	1006.43
Aluminum	2719	-	202.4	871

Airflow in the duct is presumed to be subsonic, turbulent and incompressible. Additionally, the steady airflow condition is also utilized for all the investigations. No slip condition is employed for the solid-fluid interface. Inlet and outlet faces are given inlet velocity and pressure outlet conditions respectively whereas, the base wall and side walls of the fluid domain are considered to be completely insulated. Ambient air velocity entering the duct is evaluated by using Eq. (7) and varying the Re from 3000 to 18000 with each increment of 3000. A constant gauge pressure of zero pascals normal to the boundary is applied to the outlet face.

Table 3.4 Boundary conditions

Boundary Name	Boundary Condition
Inlet face	Velocity inlet, (0.94-5.69) m/s, 300 K
Outlet face	Pressure outlet, zero-gauge pressure
Bottom and side duct walls	No slip
Absorber top surface	No slip, 1000 W/m <sup>2</sup>

Table 3.4 depicts an overview of boundary conditions used. The SIMPLE algorithm is employed for pressure-velocity coupling. To observe convergence in results, a criterion with residuals of the order of  $10^{-6}$  and  $10^{-3}$  has been set for energy and all other equations respectively.

## **Summary**

This chapter discusses the methodology followed to complete the 3-D analysis of the proposed solar air collector design. Details on the design of geometry including but not limited to absorber and impingement plates are provided. Additionally, the chapter deliberates on how the computational domain consisting of air as a fluid zone and aluminum plate as a solid zone is considered and discretized into an unstructured fine mesh. Moreover, grid independence test results, boundary conditions and solution methods are also elaborated on in detail.

## References

- [1] ASHARE Standard 93–97, Method of Testing to Determine the Thermal Performance of Solar Collector. 1977.
- [2] A. Kumar and M. H. Kim, “Effect of roughness width ratios in discrete multi V-rib with staggered rib roughness on overall thermal performance of solar air channel,” *Sol. Energy*, vol. 119, pp. 399–414, 2015, doi: 10.1016/j.solener.2015.06.030.
- [3] S. K. Sharma and V. R. Kalamkar, Computational Fluid Dynamics approach in thermo-hydraulic analysis of flow in ducts with rib roughened walls - A review, vol. 55. Elsevier, 2016.
- [4] A. S. Yadav, A. Mishra, K. Dwivedi, A. Agrawal, A. Galphat, and N. Sharma, “Investigation on performance enhancement due to rib roughened solar air heater,” *Mater. Today Proc.*, vol. 63, pp. 726–730, 2022, doi: 10.1016/j.matpr.2022.05.071.
- [5] A. D. Gupta and L. Varshney, “Performance prediction for solar air heater having rectangular sectioned tapered rib roughness using CFD,” *Therm. Sci. Eng. Prog.*, vol. 4, pp. 122–132, 2017, doi: 10.1016/j.tsep.2017.09.005.
- [6] R. Chauhan and N. S. Thakur, “Heat transfer and friction factor correlations for impinging jet solar air heater,” *Exp. Therm. Fluid Sci.*, vol. 44, pp. 760–767, 2013, doi: 10.1016/j.expthermflusci.2012.09.019.

# Chapter 4

## Results and Discussions

### 4.1. Validation of the numerical model

#### 4.1.1. Validation with smooth rectangular air channel

Validation of the results for the proposed model is carried out by comparing results from numerical analysis with correlations from the literature. Firstly, the Dittus Boelter equation [1] and Blasius equation [2] is used for estimating the Nu and ff respectively for smooth rectangular air channel for the given range of Re.

$$Nu_{smooth} = 0.023 \times (Re)^{0.8} \times (Pr)^{0.4} \quad (10)$$

$$ff_{smooth} = 0.085 \times (Re)^{-0.25} \quad (11)$$

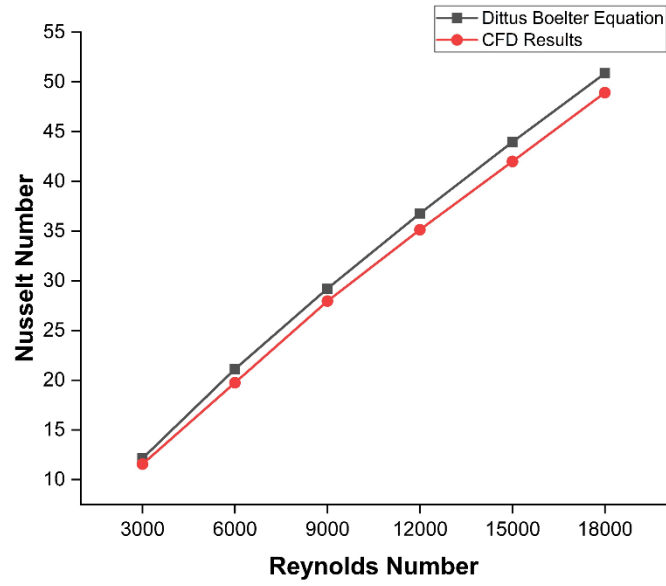
Analysis results for the smooth absorber without any ribs and impingement for similar boundary conditions are evaluated. An analogy between Nu and ff obtained from the numerical examinations with that predicted from the Eqs (10) and (11) has been drawn in Fig. 4.1. It can be observed that analysis for both Nu and ff exhibit good agreements with the predicted results from mathematical equations with average deviations of 5.1% and 5.3% respectively.

#### 4.1.2. Validation with impinging air jets onto a smooth absorber

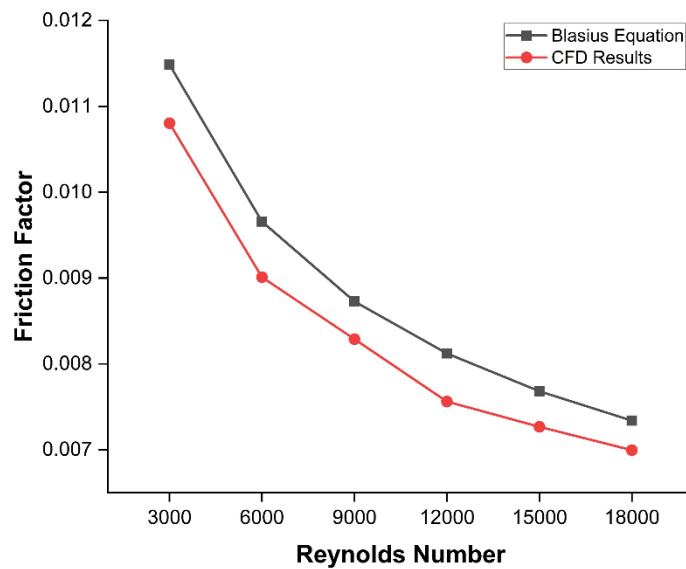
The second validation is carried out by using correlations developed by Chauhan and Thakur [3] for air impingement onto a smooth absorber.

$$Nu_{imp} = 1.658 \times 10^{-3} \times Re^{0.8512} \left(\frac{X_j}{D_h}\right)^{0.1761} \left(\frac{Y_j}{D_h}\right)^{0.141} \left(\frac{D_j}{D_h}\right)^{-1.9854} \\ \times \exp\left[-0.3498 \left(\ln\left(\frac{D_j}{D_h}\right)\right)^2\right] \quad (12)$$

$$ff_{imp} = 0.3475 \times Re^{-0.5244} \left(\frac{X_j}{D_h}\right)^{0.4169} \left(\frac{Y_j}{D_h}\right)^{0.5321} \left(\frac{D_j}{D_h}\right)^{-1.4848} \\ \times \exp\left[-0.2210 \left(\ln\left(\frac{D_j}{D_h}\right)\right)^2\right] \quad (13)$$



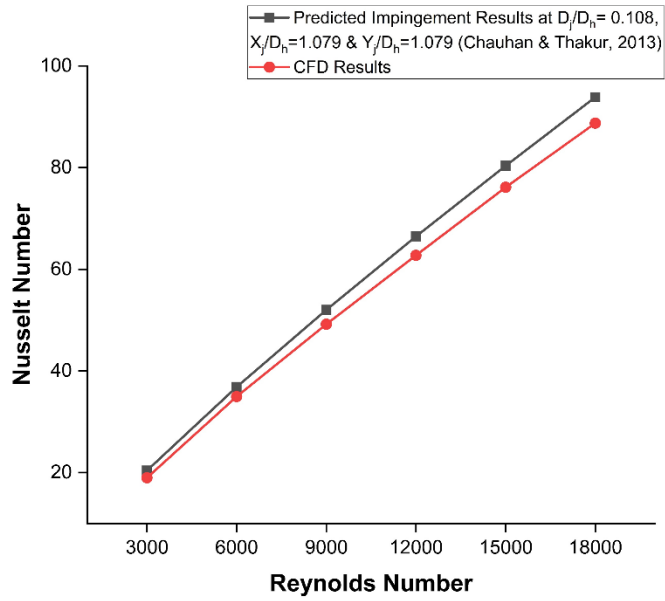
(a)



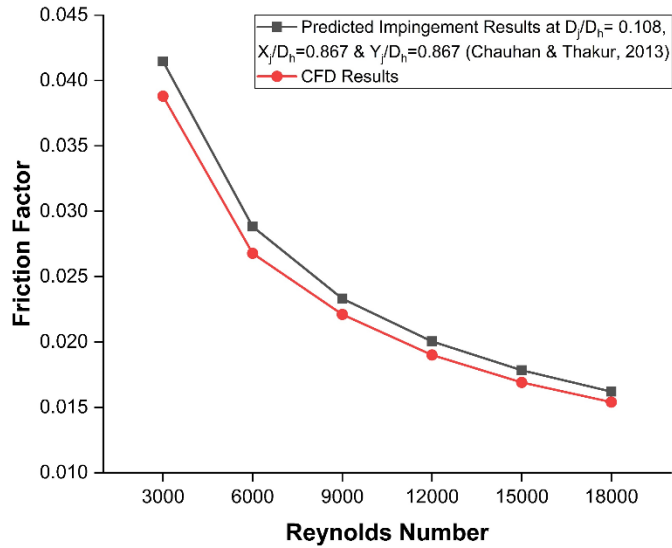
(b)

Fig. 4.1 (a) Nu validation against Dittus Boelter equation (b) ff validation against Blasius equation

This time results obtained from numerical analysis of smooth absorber with air impingement configuration ( $D_j/D_h$ ,  $X_j/D_h$  and  $Y_j/D_h$  fixed to 0.108, 0.867 and 0.867 respectively) and without any ribs are extracted for similar boundary conditions in the form of Nu and ff. Fig. 4.2 (a) and Fig. 4.2 (b) outline that analysis results for smooth absorber with air impingement are consistent with Nu and ff data calculated from Eqs, (12) and (13) with average deviations of 5.64% and 4.53% respectively.



(a)



(b)

Fig. 4.2 (a) Nu validation against impingement correlation (b) ff validation against impingement correlation

## 4.2. Effect on temperature distribution

Analysis outcomes in terms of temperature distribution for smooth absorber at  $Re = 12000$  have been presented in Fig. 4.3 (a) whereas temperature distribution for the proposed combined configuration of rectangular sectioned V-ribs ( $e/D_h = 0.020$ ,  $P/D_h = 0.528$  and  $\alpha = 60^\circ$ ) and air impingement ( $D_j/D_h$ ,  $X_j/D_h$  and  $Y_j/D_h$  fixed to 0.108, 0.867 and 0.867 respectively) has been depicted in Fig. 4.3 (b) respectively under similar flow conditions. From Fig. 4.3, it can be clearly established that temperature distribution in the duct having rectangular sectioned V-ribs and air impingement

configuration is more developed as compared to a smooth duct having no roughness and impingement arrangement. To explain, in contrast to the smooth absorber surface temperature, the temperature of the artificially roughened plate with air impinging on its lower surface is lower. This phenomenon can be attributed to the combined cooling effect of rectangular sectioned V-ribs and air impingement in the latter arrangement. And subsequently, this cooling effect augments the heat transfer.

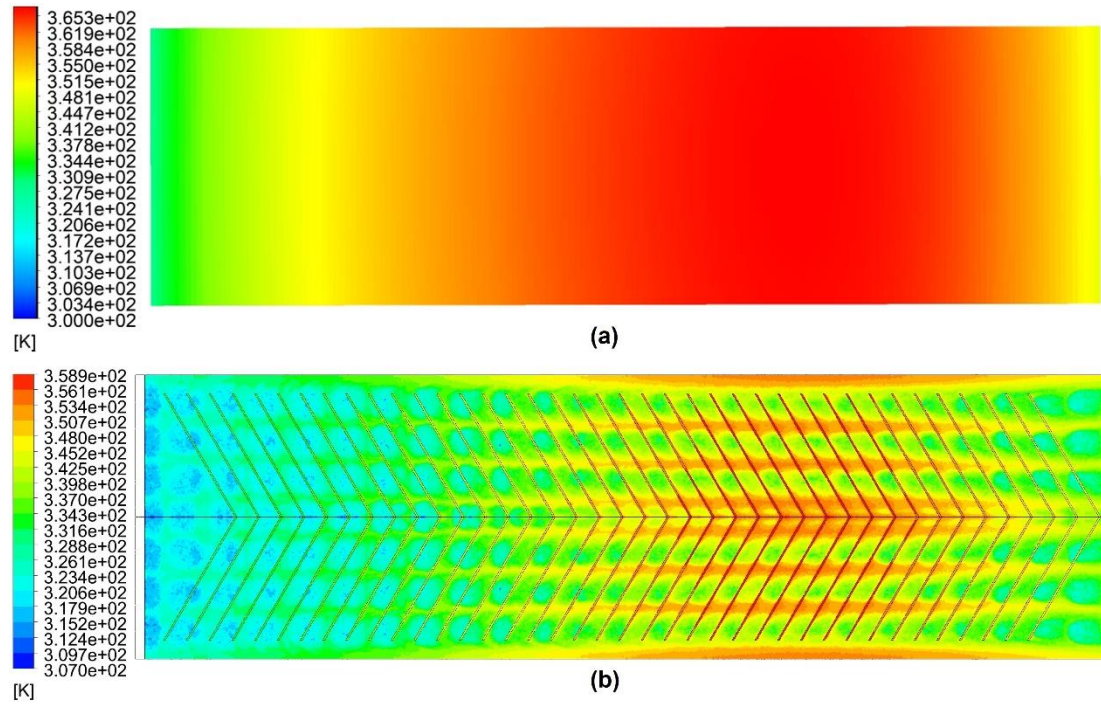


Fig. 4.3 Temperature distribution at  $Re = 12000$  on test section of (a) smooth absorber (b) absorber with rectangular sectioned V-ribs

### 4.3. Effect on Nusselt number

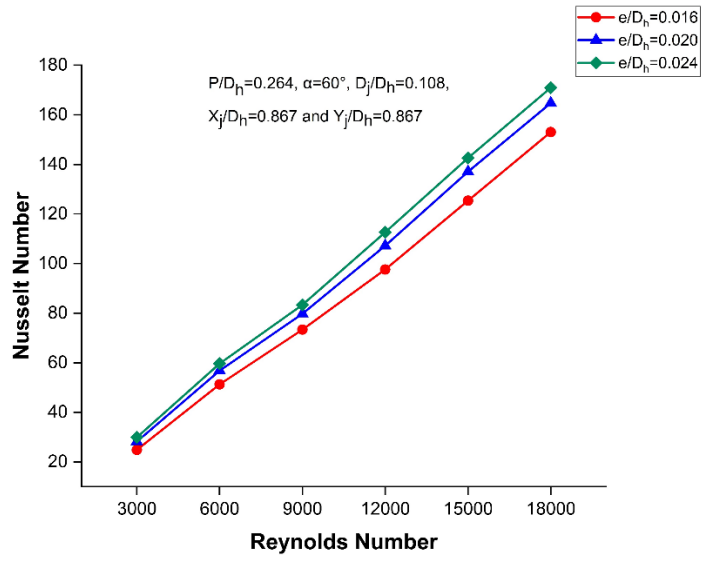
The variation of  $Nu$  as a function of  $Re$  for fixed values of impingement parameters at varying  $e/D_h$ ,  $P/D_h$  and  $\alpha$  respectively is shown in Fig. 4.4. It can be assimilated from the graphical data that in all the cases  $Nu$  behaves predictably and rises predominantly as  $Re$  is increased from 3000 to 18000. The phenomenon can be referred to as the separation of the boundary layer with the increasing flow rate which in turn inevitably gives rise to heat transfer. Fig. 4.5 illustrates this phenomenon in the form of contours of Turbulent kinetic energy (TKE) in the plane normal to the absorber surface and parallel to the flow direction. More secondary vortices are formed near the area where air jets strike the rectangular sectioned ribs having the configuration  $e/D_h = 0.020$ ,  $P/D_h = 0.528$ ,  $\alpha = 60^\circ$  at higher Reynolds numbers and thus a substantial rise in  $Nu$  is observed.



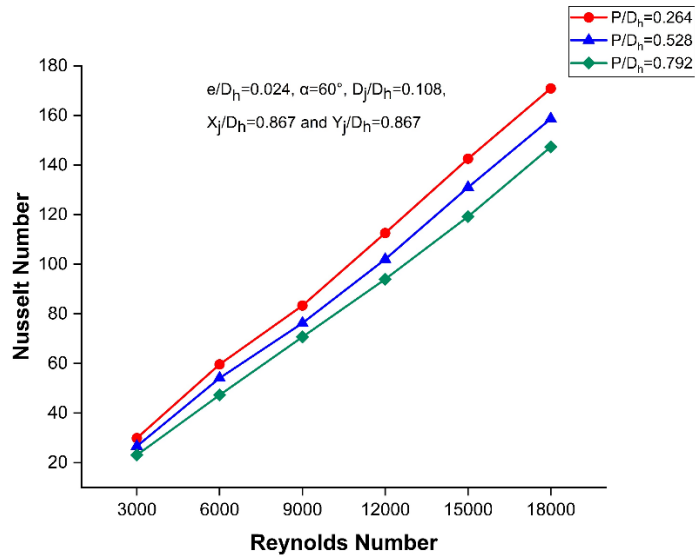
The influence of varying  $e/D_h$  at constant values  $P/D_h = 0.264$  and  $\alpha = 60^\circ$  on Nu for the given range of Re has been discussed in the form of graphical data in Fig. 4.4 (a). Impingement parameters are kept constant. It can be interpreted from the results that the repercussions of expanding  $e/D_h$  are in favor of heat transfer with Nu continuously improving as the value of  $e/D_h$  increases from 0.016 to 0.024 for the given range of Re from 3000 to 18000. This improvement in heat transfer is associated with the fact that rectangular sectioned V-ribs with longer roughness height induce more turbulence in the path of airflow causing air to extract more heat from the absorbing surface. Hence,  $e/D_h = 0.024$  produces a maximum value of Nu at  $Re = 18000$  among its lower values. Ravi and Saini [4] analyzed the effect of relative rib size on heat transfer characteristics and found that longer rib size strongly encourages secondary flow.

Similarly, Fig. 4.4 (b) shows the effect of varying  $P/D_h$  for fixed  $e/D_h = 0.024$  and  $\alpha = 60^\circ$  on Nu for the considered range of Re. Again, impingement parameters are kept constant. Furthermore, enhancing  $P/D_h$  depreciates heat transfer with rectangular sectioned V-ribs having the smallest value of  $P/D_h = 0.264$  showcasing the best heat transfer characteristics among its higher values of 0.528 and 0.792 at a flow rate ranging from 3000 to 18000. In simpler words, a lower relative roughness pitch means fewer gaps among ribs in the given length of the absorber which insinuates early flow separation and encourages the formation of secondary flow vortices in the incoming jet flow from the impingement plate.

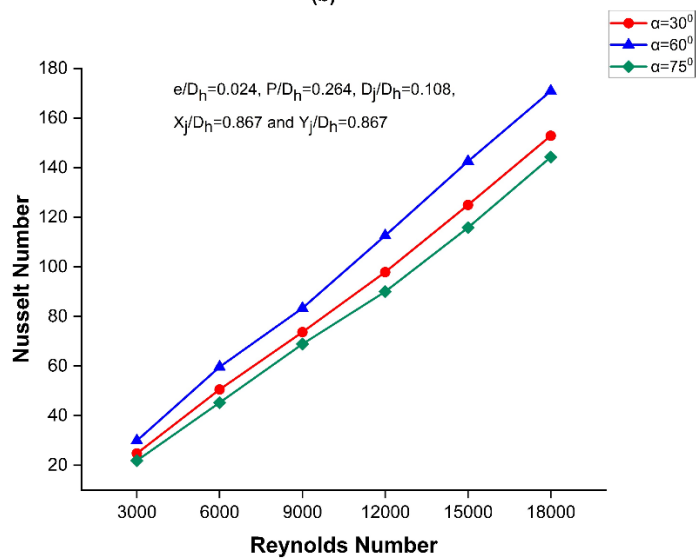
Change in Nu at different values of Re with varying angle of attack of flow ( $\alpha$ ) parameter for rectangular sectioned V-ribs has been presented in Fig. 4.4 (c) at fixed values of  $e/D_h$  and  $P/D_h$  for 0.024 and 0.264 respectively. It can be noted that the effects of varying  $\alpha$  on heat transfer are more significant than that of varying  $e/D_h$  and  $P/D_h$ . The results clearly reflect Nu augments as  $\alpha$  enhances from  $30^\circ$  to  $60^\circ$  but diminishes remarkably as  $\alpha$  reaches  $75^\circ$  and shows a maximum value of Nu at  $\alpha = 60^\circ$  and  $Re = 18000$ . This fluctuation in Nu with respect to  $\alpha$  is characteristically similar to that reported by Momin et al. [5].



(a)



(b)



(c)

Fig. 4.4 Change in Nu against Re as a function of (a)  $e/D_h$  (b)  $P/D_h$  and (c)  $\alpha$

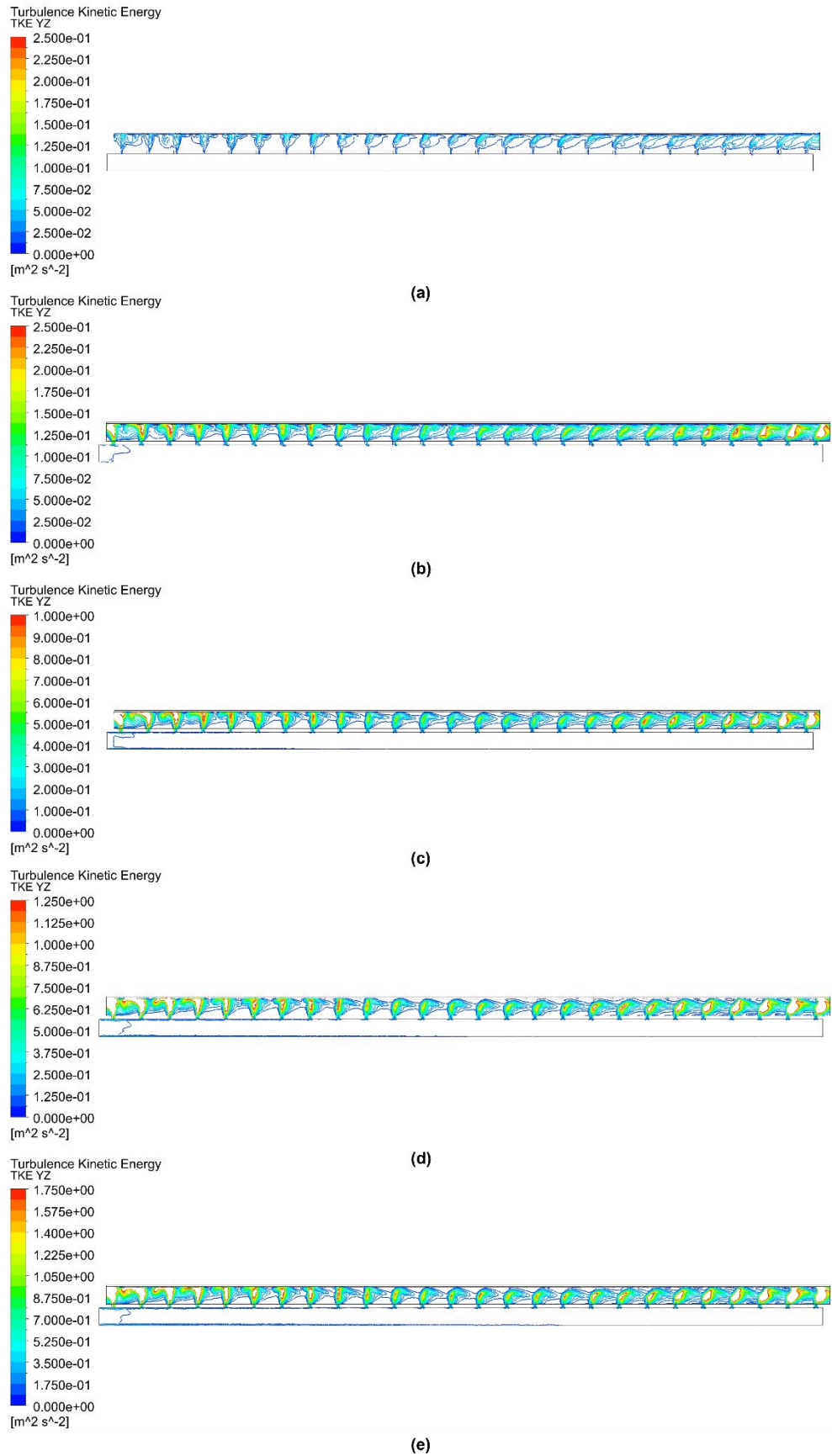


Fig. 4.5 Contours of Turbulent kinetic energy at  $e/D_h = 0.020$ ,  $P/D_h = 0.528$ ,  $\alpha = 60^\circ$  for Re (a) 3000 (b) 6000 (c) 12000 (d) 15000 (e) 18000

In addition, a comparison of results obtained from numerical analysis in terms of Nu with the parallel flow and previous studies for air impingement [3] and V-shaped rib roughness [5] under similar conditions of airflow (3000-18000) has been drawn. This comparison can be visualized in Fig. 4.6 to evaluate the effect of air impingement and rectangular sectioned V-ribs (present study) on heat transfer improvement. Impingement parameters of  $D_j/D_h = 0.108$ ,  $X_j/D_h = 0.867$  and  $Y_j/D_h = 0.867$  whereas roughness parameters of  $e/D_h = 0.024$ ,  $P/D_h = 0.264$  and  $\alpha = 60^\circ$  are used. It can be determined that the combined configuration of rectangular sectioned V-ribs with air impingement thermally outperforms its corresponding configurations of parallel flow, air impingement (without ribs) and V-shaped ribs (without impingement). Furthermore, the present study with roughness configuration of  $e/D_h = 0.024$ ,  $P/D_h = 0.264$ ,  $\alpha = 60^\circ$  and impingement configuration of  $D_j/D_h$ ,  $X_j/D_h$  and  $Y_j/D_h$  fixed to 0.108, 0.867 and 0.867 respectively exhibits maximum enhancement in Nu of factor 3.36, 2.06 and 1.82 at  $Re = 18000$  as compared to parallel flow, air impingement (without ribs) and V-shaped ribs (without impingement).

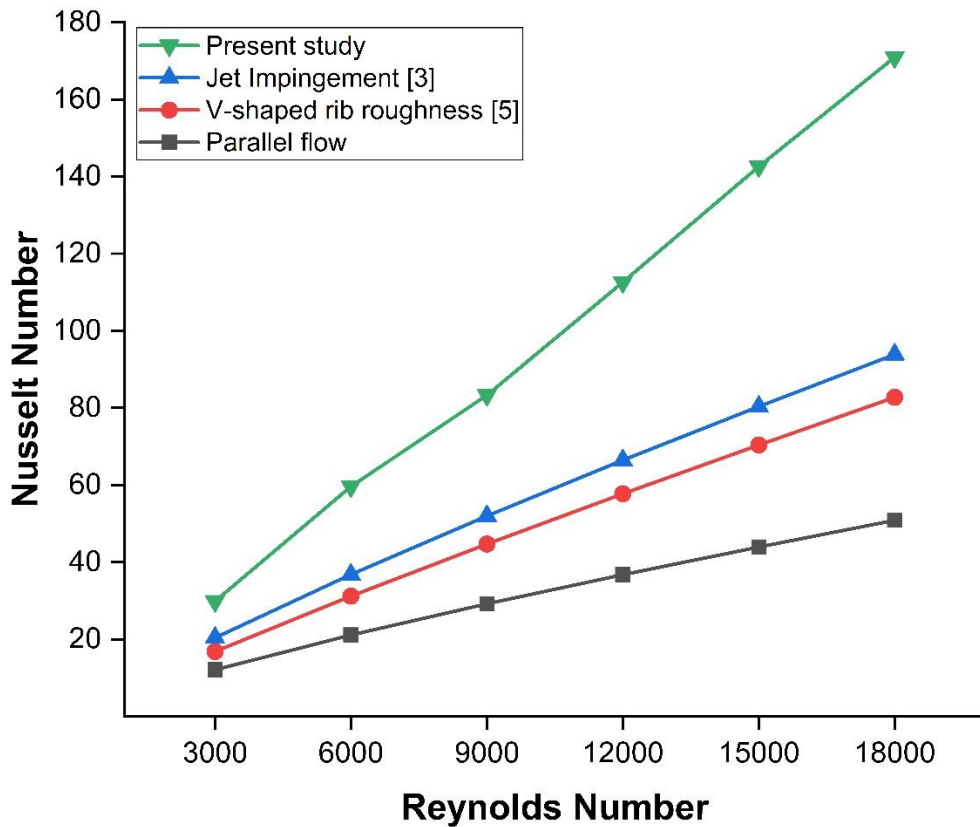


Fig. 4.6 Comparison of Nu with literature at various values of Re

Fundamentally, it can be conceptualized that this enhancement in Nu is nothing but a mere result of two paramount interactions of air. These two interactions occur simultaneously and can be assimilated from the contours of TKE for  $Re = 9000$  in the YZ direction for the configuration  $e/D_h = 0.020$ ,  $P/D_h = 0.528$ ,  $\alpha = 60^\circ$  in Fig. 4.7. Air impingement being the first interaction where air jets strike the absorber bottom surface and impart a secondary flow to the air near absorber surface. Second is the interaction of this flow with the ribs where this flow further disintegrates into two flows. One flow recycles the rib section in the form of secondary vortices whereas the other mixes with the mainstream flow. Similar repercussions of variation of Turbulent kinetic energy on Nu are reported by Gupta and Varshney [6].

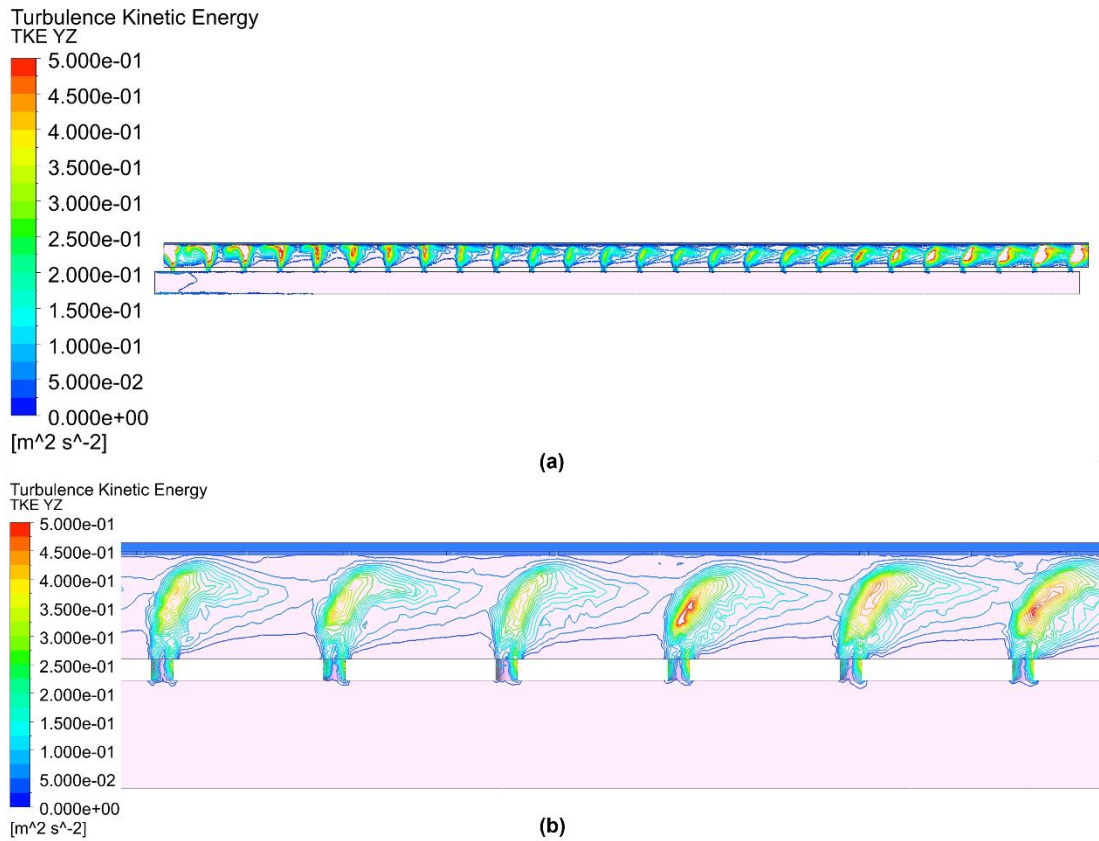


Fig. 4.7 Contours of Turbulent kinetic energy at  $Re = 9000$  at  $e/D_h = 0.020$ ,  $P/D_h = 0.528$ ,  $\alpha = 60^\circ$  (a) Test section (b) enlarged view

#### 4.4. Effect on friction factor

A detailed examination of results for pressure drop with respect to  $Re$  has been presented in Fig. 4.8 in the form of plots of  $ff$  against  $Re$  for varying  $e/D_h$ ,  $P/D_h$  and  $\alpha$  respectively. It may be noted that the velocity of airflow in the duct has an inverse relation with  $ff$  therefore an increase in the value of  $Re$  is accompanied by a gradual

decrease in friction factor and a minimum value of  $ff$  of 0.036 is achieved at  $e/D_h = 0.024$ ,  $P/D_h = 0.264$ ,  $\alpha = 75^\circ$  and  $Re = 18000$ . Moreover, the influence of expanding  $e/D_h$  on  $ff$  for the range of  $Re$  by keeping  $P/D_h$  and  $\alpha$  constant has been illustrated in Fig. 4.8 (a). The data shows that pressure drop across the duct increases as rib height ( $e/D_h$ ) increases and is highest when  $e/D_h = 0.024$ . This can be related to the fact that greater interruptions in the flow of air constitute a greater pressure drop across the duct. The influence of increasing the gap ( $P/D_h$ ) between the two ribs on  $Nu$  has been depicted for fixed  $e/D_h$  and  $\alpha$  in Fig. 4.8 (b). The  $ff$  plot against  $Re$  describes that as  $P/D_h$  increases,  $ff$  diminishes and achieves the lowest value at  $P/D_h = 0.792$ . These findings are in agreement with the study conducted by Yadav and Bhagoria [7] on square-sectioned transverse ribs. The data in Fig. 4.8 (c) represents the effect of varying  $\alpha$  parameters at fixed values of  $e/D_h$  and  $P/D_h$  for 0.024 and 0.264 respectively. It can be seen from the graphical data that  $ff$  initially rises as  $\alpha$  is increased from  $30^\circ$  to  $60^\circ$  but decreases to a new minimum value at  $60^\circ$  for the given  $Re$ . This fluctuation in  $ff$  with respect to  $\alpha$  is similar in nature to the one reported by Momin et al. [5].

The combined effect of rectangular sectioned V-ribs and air impingement on flow characteristics has been analyzed with respect to parallel flow, air impingement [3] and V-shaped rib roughness [5] in Fig. 4.9. It is clear that the present study with the roughness configuration of  $e/D_h = 0.024$ ,  $P/D_h = 0.264$ ,  $\alpha = 60^\circ$  and impingement configuration of  $D_j/D_h$ ,  $X_j/D_h$  and  $Y_j/D_h$  fixed to 0.108, 0.867 and 0.867 respectively demonstrate maximum improvement in  $ff$  of factor 5.31, 3.49 and 2.55 at  $Re = 18000$  as compared to parallel flow, air impingement (without ribs) and V-shaped ribs (without impingement) respectively.

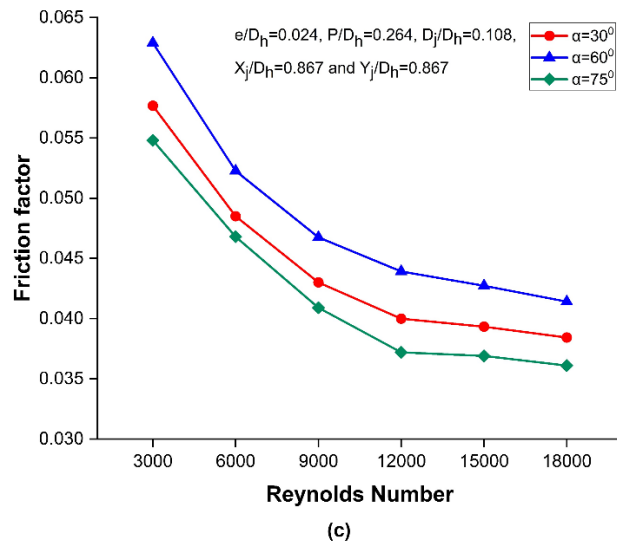
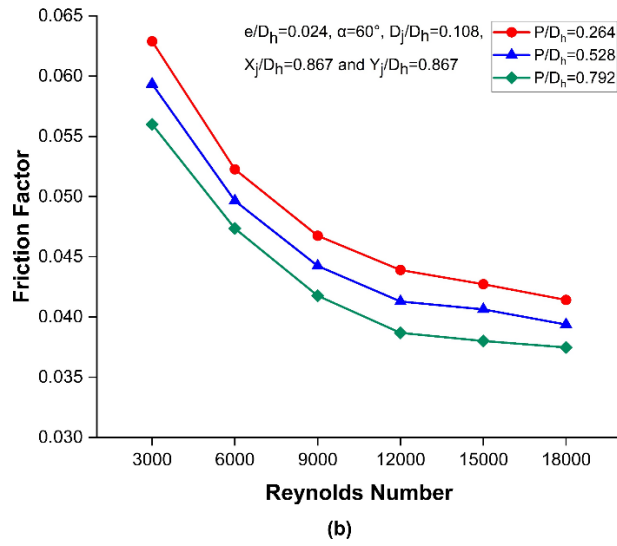
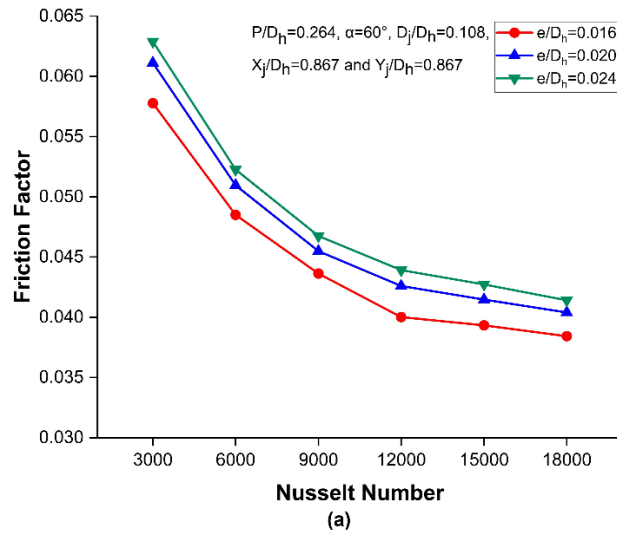


Fig. 4.8 Change in ff against Re as a function of (a)  $e/D_h$  (b)  $P/D_h$  and (c)  $\alpha$

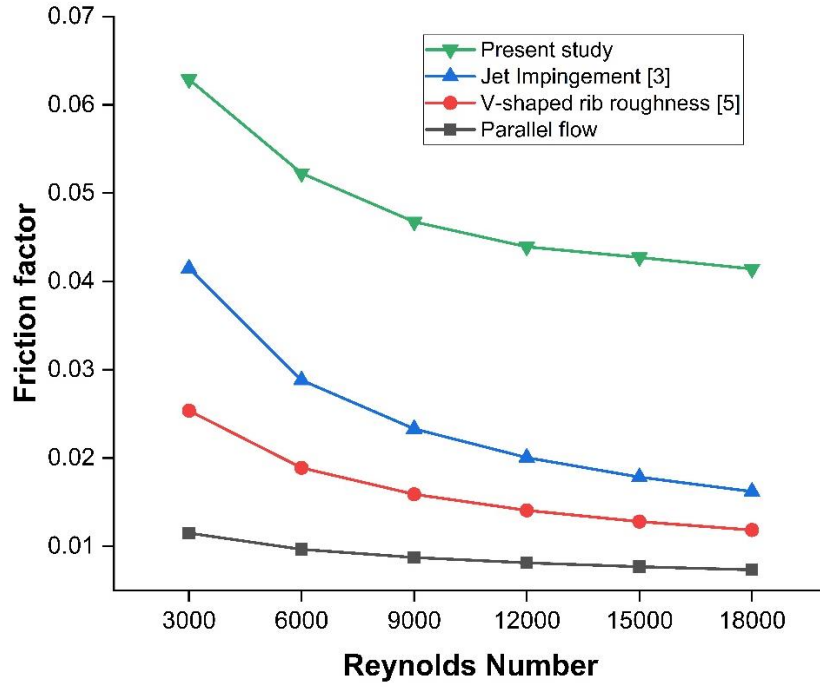


Fig. 4.9 Comparison of ff with literature at various values of Re

#### 4.5. Effect on thermohydraulic performance( $\eta_{combined}$ )

Despite an ample thermal improvement in using the combined arrangement of air impingement with rectangular sectioned V-ribs as shown in Fig. 4.6 a substantial rise in the pressure (pumping power) to overcome the turbulence in the SAH is also observed and is shown in Fig. 4.8. Subsequently, it is equally important to analyze the thermohydraulic performance( $\eta_{combined}$ ) of the SAH and to find the optimal parameters at which a favorable compensation between heat transfer improvement and friction factor penalty can be accomplished. Momin et al. [5] evaluated the thermohydraulic performances using a mathematical relation similar to Eq (7).

$$\eta_{combined} = \frac{Nu_{combined} / Nu_{smooth}}{(ff_{combined} / ff_{smooth})^{\frac{1}{3}}} \quad (14)$$

Fig. 4.10 represents the graphical data as a result of thermohydraulic analysis of the combined arrangement of air impingement with rectangular sectioned V-ribs. It can be deduced that  $\eta_{combined}$  is greater than unity and it further strengthens as the value of Re increases from 3000 to 18000 for all the examinations. Moreover, Fig. 4.10 (a), Fig. 4.10 (b) and Fig. 4.10 (c) indicate that  $\eta_{combined}$  achieves a maximum value of 1.92 at  $e/D_h = 0.024$ ,  $P/D_h = 0.264$ ,  $\alpha = 60^\circ$  and  $Re = 18000$  and that  $\alpha$  among other parameters of roughness affects system performance the most.



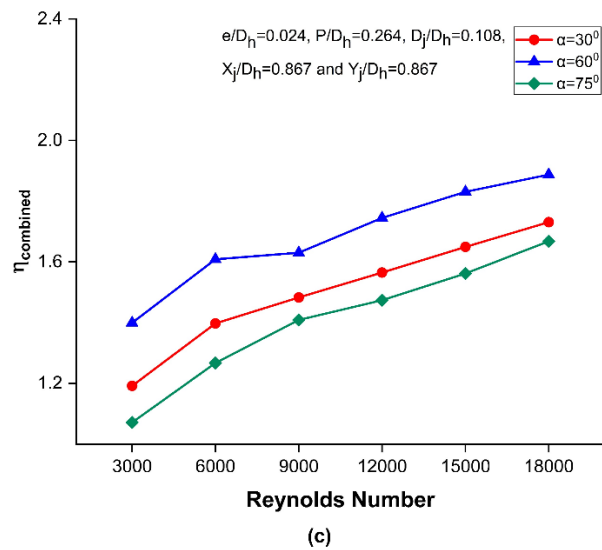
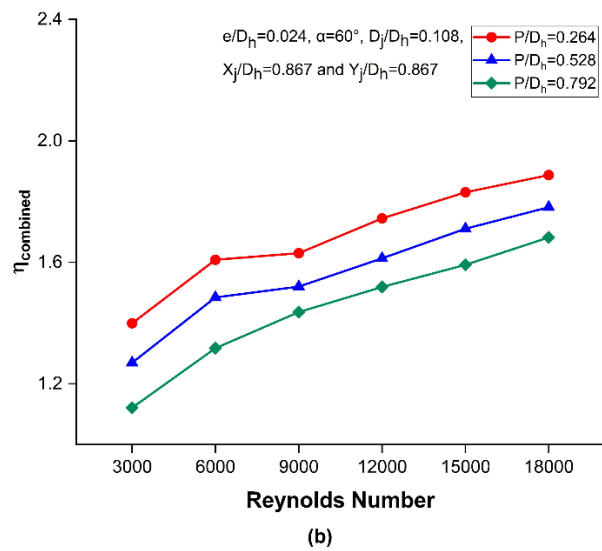
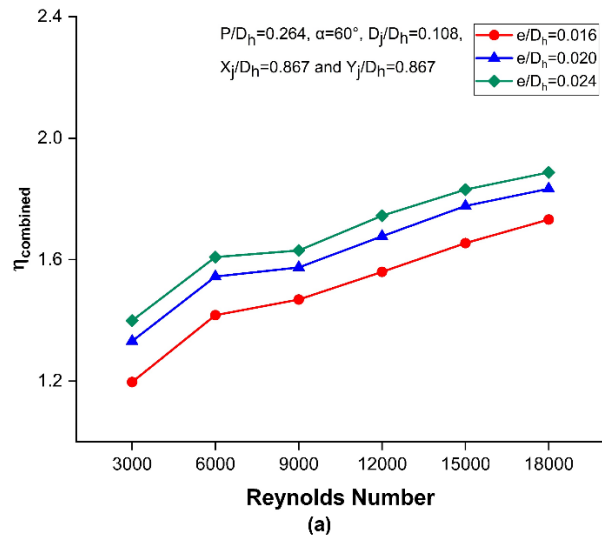


Fig. 4.10 Change in  $\eta_{combined}$  against Re as a function of (a)  $e/D_h$  (b)  $P/D_h$  and (c)  $\alpha$

## Summary

This chapter discusses the validation of the numerical model from past literature studies. Numerical investigations on a rectangular solar air heater having a combined configuration of rectangular sectioned V-ribs on the lower surface of the absorber and air impingement from the lower channel have been performed in this study. Results from the numerical analysis have been discussed in the graphical form of Nu and ff against the range of flow parameters from 3000 to 18000 for different roughness parameters  $e/D_h$ ,  $P/D_h$ , and  $\alpha$ . Comparisons of Nu and ff between the present work and conventional SAH have been drawn under similar flow conditions. Moreover, the thermohydraulic performance of the proposed configurations has been discussed to find optimal roughness parameters.

## References

- [1] D. B. Spalding, Handbook of heat transfer, vol. 18, no. 10. 1975.
- [2] M. S. Bhatti and R. K. Shah, Turbulent and Transition Convective Heat Transfer in Ducts. Wiley, New York, 1987.
- [3] R. Chauhan and N. S. Thakur, “Heat transfer and friction factor correlations for impinging jet solar air heater,” *Exp. Therm. Fluid Sci.*, vol. 44, pp. 760–767, 2013, doi: 10.1016/j.expthermflusci.2012.09.019.
- [4] R. K. Ravi and R. P. Saini, “Nusselt number and friction factor correlations for forced convective type counter flow solar air heater having discrete multi V shaped and staggered rib roughness on both sides of the absorber plate,” *Appl. Therm. Eng.*, vol. 129, pp. 735–746, 2018, doi: 10.1016/j.applthermaleng.2017.10.080.
- [5] A.-M. E. Momin, J. S. Saini, and S. C. Solanki, “Heat transfer and friction in solar air heater duct with V-shaped rib roughness on absorber plate,” *Energy*, vol. 36, no. 7, pp. 4531–4541, 2002, doi: 10.1016/j.energy.2011.03.054.
- [6] A. D. Gupta and L. Varshney, “Performance prediction for solar air heater having rectangular sectioned tapered rib roughness using CFD,” *Therm. Sci. Eng. Prog.*, vol. 4, pp. 122–132, 2017, doi: 10.1016/j.tsep.2017.09.005.
- [7] A. S. Yadav and J. L. Bhagoria, “A numerical investigation of square sectioned transverse rib roughened solar air heater,” *Int. J. Therm. Sci.*, vol. 79, pp. 111–131, 2014, doi: 10.1016/j.ijthermalsci.2014.01.008.

# Chapter 5

## Conclusions and Future Recommendations

### 5.1. Conclusions

In this study, the repercussions of impinging air jets onto an absorber having rectangular sectioned V-ribs on its bottom surface in terms of Nu and ff and  $\eta_{\text{combined}}$  are determined using a 3D numerical analysis. The variation of each roughness parameter i.e.,  $e/D_h$ ,  $P/D_h$ , and  $\alpha$  against the range of Re from 3000 to 18000 have been numerically examined at fixed values of impingement parameters to estimate their corresponding efficacy on Nu and ff and  $\eta_{\text{combined}}$ . The findings of this study can be summarized in the following points:

- The novel geometry of SAH having rectangular sectioned V-ribs as artificial roughness integrated with impingement cooling configuration compliments heat transfer and temperature distribution.
- Nu shows an increasing tendency against increasing Re, whereas ff depreciates as Re increases. Nu achieves a peak value at Re = 18000 while ff diminishes to its lowest value at Re = 18000.
- $e/D_h = 0.024$ ,  $P/D_h = 0.264$  and  $\alpha = 60^\circ$  exhibit the highest Nu of 170.91 at Re = 18000 while  $e/D_h = 0.016$ ,  $P/D_h = 0.792$  and  $\alpha = 75^\circ$  display minimum ff value of 0.0361 at Re = 18000.
- As compared to the parallel flow, the combined effect of air impingement and rectangular sectioned V-ribs showcase maximum enhancements in Nu and ff of the order 3.36 and 5.31 respectively at Re = 18000 and  $e/D_h = 0.024$ ,  $P/D_h = 0.264$ ,  $\alpha = 60^\circ$ .
- $\eta_{\text{combined}}$  greater than unity for all the considered configurations clearly indicates the performance efficacy of the combined arrangement of impinging air jets onto rectangular sectioned V-ribs.
- Maximum  $\eta_{\text{combined}}$  of the factor 1.92 is accomplished at  $e/D_h = 0.024$ ,  $P/D_h = 0.264$ ,  $\alpha = 60^\circ$  for Re = 18000.

- The proposed arrangement of rectangular sectioned V-ribs with assimilation of impingement cooling configuration is an effective way of augmenting the performance of SAHs.

## **5.2. Future Recommendations**

The following recommendations are suggested that can be investigated to further augment the heat transfer and fluid flow characteristics in solar air heaters.

- A study incorporating the design of V-shaped roughness with gap rib in an impinging jet solar air heater.
- A study incorporating the design of discrete V-shaped rib roughness in an impinging jet solar air heater.
- A study comparing the performances of all the V-shaped roughness configurations including the rectangular sectioned V-shaped rib roughness (used in this study) in an impinging jet solar air heater.

## **Acknowledgments**

All praise and gratitude be to Allah, the Almighty, who endowed me with the ability to grasp, learn, and finish my thesis report.

I would like to take this opportunity to offer my heartfelt appreciation to my supervisor, Dr. Majid Ali, and co-supervisor, Dr. Naveed Ahmed, for their invaluable insights, knowledge, and support over the course of this project. I would also like to acknowledge my GEC members Dr. Adeel Waqas, Dr. Mariam Mahmood, and Dr. Muhammad Bilal Sajid for guiding me throughout the project. Moreover, I would also like to thank my family and friends, particularly Muhammad Rehan Iqbal, Ayesha Iqbal, and Muhammad Ahmed, for their constant motivation and support.

## **Appendix I: Research Article**

### **Title**

Numerical analysis of a solar air heater having rectangular sectioned V-ribs as artificial roughness integrated with impingement cooling configuration

### **Abstract**

The application of solar air heaters (SAHs) is an effective method of utilizing abundant solar energy for heating purposes and reducing the consumption of fossil fuels. However, the performance of SAHs is characteristically low owing to a sublayer formation over the heated surface. To address this low performance, numerical examinations on a novel configuration of SAH have been performed in this study. The proposed design encompasses a combined arrangement of both impinging air jets and rectangular sectioned V-ribs on the absorber surface. A validated numerical model is used to investigate the effect of varying roughness height, pitch, and angle of attack from 0.016 to 0.024, 0.264 to 0.792, and 30° to 75° respectively while keeping impingement parameters fixed and varying Re from 3000 to 18000. The analysis results in terms of Nusselt number (Nu) and friction factor (ff) characteristics as a function of roughness parameters are evaluated. The results exhibit a considerable enhancement of 3.36 and 5.31 in Nu and ff respectively in contrast to conventional SAHs under similar boundary conditions. Moreover, the proposed model performs best at Re = 18000 with the highest thermohydraulic performance ( $\eta_{\text{combined}}$ ) of 1.92. The presented results conclude that the proposed arrangement of jet cooling with rectangular sectioned V-ribs is an efficacious way for improving the performance of SAHs.

### **Journal Name**

Sustainable Energy Technologies and Assessments (Under Review)

### **Authors**

Muhammad Haroon Iqbal, Naveed Ahmed, Majid Ali, Mumtaz A Qaisrani, Mariam Mahmood, Adeel Waqas, Muhammad Bilal Sajid

← Submissions Being Processed for Author

Page: 1 of 1 (1 total submissions)

Results per page 10

Action	Manuscript Number	Title	Initial Date Submitted	Status Date	Current Status
<a href="#">View Submission</a> <a href="#">Send E-mail</a>	SETA-D-23-00061	Numerical analysis of a solar air heater having rectangular sectioned V-ribs as artificial roughness integrated with impingement cooling configuration	Jan 06, 2023	Jan 10, 2023	Under Review

Page: 1 of 1 (1 total submissions)

Results per page 10



